

Department of Physics and Astronomy

University of Heidelberg

Master thesis

in Physics

submitted by

Elsa Wilken

born in Hamburg

2018

**Retrieval advances of BrO/SO₂ molar ratios from
NOVAC**

This Master thesis has been carried out by Elsa Wilken
at the
Institute for Environmental Physics, University of Heidelberg,
Germany
under the supervision of
Prof. Ulrich Platt

(Titel der Masterarbeit - deutsch):

(Abstract in Deutsch)

Lorem ipsum dolor sit amet, consectetur adipisici elit, sed eiusmod tempor incididunt ut labore et dolore magna aliqua. Ut enim ad minim veniam, quis nostrud exercitation ullamco laboris nisi ut aliquid ex ea commodo consequat. Quis aute iure reprehenderit in voluptate velit esse cillum dolore eu fugiat nulla pariatur. Excepteur sint obcaecat cupiditat non proident, sunt in culpa qui officia deserunt mollit anim id est laborum.

Duis autem vel eum iriure dolor in hendrerit in vulputate velit esse molestie consequat, vel illum dolore eu feugiat nulla facilisis at vero eros et accumsan et iusto odio dignissim qui blandit praesent luptatum zzril delenit augue duis dolore te feugait nulla facilisi. Lorem ipsum dolor sit amet, consectetur adipisciing elit, sed diam nonummy nibh euismod tincidunt ut laoreet dolore magna aliquam erat volutpat.

Ut wisi enim ad minim veniam, quis nostrud exerci tation ullamcorper suscipit lobortis nisl ut aliquip ex ea commodo consequat. Duis autem vel eum iriure dolor in hendrerit in vulputate velit esse molestie consequat, vel illum dolore eu feugiat nulla facilisis at vero eros et accumsan et iusto odio dignissim qui blandit praesent luptatum zzril delenit augue duis dolore te feugait nulla facilisi.

Retrieval advances of BrO/SO₂ molar ratios from NOVAC:

Measurements of magnitude and composition of volcanic gas emissions allow insights in magmatic processes. Within the Network for Observation of Volcanic and Atmospheric Change(NOVAC) automatically scanning UV-spectrometers are monitoring gas emission at volcanoes. The emissions of BrO and SO₂ can be retrieved from the recorded spectra by applying Differential Optical Absorption Spectroscopy(DOAS) and comparing the optical absorption of the volcanic plume to the background. Therefore, the background spectrum must not be affected by volcanic influence. Classically, the background spectrum is taken from the same scan but from a elevation angle which has been identified to be outside of the volcanic plume. However, experience shows those background spectra can still be contaminated by volcanic gases. Alternatively reference spectra can be derived from 1) a theoretical solar atlas spectrum or 2) a volcanic-gas-free reference spectrum recorded by the same instrument. 1) comes with a drawback of reduced precision, as the instrumental effects have to be modeled and added to the retrieval. For 2), the alternative reference spectrum should be recorded at similar conditions with respect to meteorology and radiation. We use the first option to check for contamination and the second to evaluate the spectra to maintain a god fit quality. We present our approach and its results when applied on NOVAC data from Tungurahua and Nevado Del Ruiz.

Contents

1	Introduction	6
I	Theoretical Background	9
1.1	Volcanism and volcanic chemistry	10
1.1.1	Volcanism	10
1.1.2	Volcanic degassing	12
1.1.3	Volcanic gases and their impact on the climate	15
1.1.4	Volcanic plume chemistry	16
1.1.5	Sulphur species	16
1.1.6	Bromine oxide	19
1.1.7	Using volcanic gases to study volcanic activity	20
1.2	Remote sensing of volcanic gases	23
1.2.1	Absorption spectroscopy	23
1.2.2	Scattering processes in the atmosphere	24
1.2.3	Differential Optical Absorption Spectroscopy(DOAS)	25
II	Evaluation of the Data of Tungurahua and Nevado Del Ruiz	31
2	Network for Observation of Volcanic and Atmospheric Change	32
2.1	Measurement Routine	33
3	Evaluation Routine	35
3.1	NOVAC-Evaluation	35
3.2	Contamination Problem	37
4	Limitations for the evaluation of BrO	42
4.1	BrO Error dependence on external parameters	42
4.1.1	Time	42
4.1.2	Temperature	44
4.1.3	Daytime	46
4.1.4	Colorindex	48
4.1.5	Elevation Angle	49
4.1.6	Exposure Time	50

5 Method	51
5.1 Fit data	52
5.2 Other approaches	55
5.2.1 Nearest neighbours	55
5.2.2 Iterative	56
6 Comparison with NOVAC Evaluation	57
7 Results	61
7.1 Tungurahua	61
7.2 Nevado Del Ruiz	61
8 Issues of our method	64
8.1 Contamination of the plume	64
9 Conclusion	65
III Appendix	66
A Lists	67
A.1 List of Figures	67
A.2 List of Tables	68
B Bibliography	69

1 Introduction

Volcanic activities on Earth have always shaped the earth surface and influenced atmospheric processes. Volcanoes are often particularly recognized by their dramatic consequences of a major volcanic eruption. But volcanoes influence our lives in more than this way. Volcanic gases can effect the weather (timescales of days to weeks) or the climate (timescales of months to years) Schmidt and Robock [2015]. Examples are the lake eruption in Iceland (1783-1784) followed by a very hot summer and a cold winter in central Europa Thordarson and Self [2003] and the Tambora eruption, indonesia in 1815 which caused the "year without summer" in 1816.

Considering the plate tectonics of earth most volcanoes are caused by diverging or converging of the continental plates and therefore located at the margins of the continental plates. Another possibility for occurrence of volcanoes is the the interior of continental or oceanic shelves. Schmincke [2000]

The most abundant volatile species released during a volcanic eruption are water vapour (H_2O ; relative amount of the plume: 50%-90%) and carbon dioxide (CO_2 ; relative amount of the plume: 1%-40%) Platt and Bobrowski [2015]. But the short effects of those two gases are rather low since there effect on atmospheric composition is negligibly due to the high abundance of atmospheric H_2O and CO_2 . But on timescales of the age of the earth the volcanic emission of H_2O and CO_2 are the source of our current atmosphere. Schmidt et al. [2015]

A typically volcanic plume consists of many different gases alongside H_2O and CO_2 sulfur dioxide (SO_2) contributes with 1%-25% to the plume, hydrogen sulfide (H_2S) with 1%-10% and hydrogen chloride with (HCl) 1%-10%. Furthermore there are trace gases for example carbon disulfide (CS_2), carbon sulfide (COS) carbon monoxide (CO) hydrogen fluoride (HF) and hydrogen bromide (HBr) Platt and Bobrowski [2015]

A decrease of stratospheric ozone (O_3) has been observed after the eruption of El Chickon in 1982 and the eruption of mount Pinatubo 1991. A depletion stratospheric O_3 results in ozone holes. The depletion comes from volcanic aerosols which serve anthropogenic chlorine/bromine into more reactive forms Solomon et al. [1998]. Volcanic gases can alter the radiative balance of the earth in timescales relevant for climate change due to scatter and absorption of solar radiation Schmidt et al. [2015]. The gas composition of the volcano plume change with activity and could be a indication for the processes inside the earth.

In this work we are particularly interested in the ratio of BrO and SO_2 . The halogen sulfur ratio is a proxy for volcanic processes. Therefore we make the assumption that the ratio of BrO and SO_2 contains informations about its degassing source

depth. A change in BrO/SO₂ prior to eruption was observed at Etna and Nevado del Ruiz.

To gain further knowledge about the volcanoes the Network for Observation of Volcanic and Atmospheric Change (NOVAC) was installed. NOVAC is a Network of DOAS Instruments located next to about 30 volcanoes in America, Africa and Europe. At every Volcano there are two to four DOAS Instruments installed, recording record back-scattered solar radiation spectra at different viewing angles.

NOVAC is a network which produces a large amount of data and we have the chance to evaluate long time periods which is a unique opportunity to study correlations of the trace gases.

Since the conditions at volcanoes are rough, the instruments need to be rather simple to keep the maintenance cheap and to assure a longer lifetime of the instruments. So we need to waive on temperature stabilization even at the expense of the quality of the data.

One possibility to measure the volcanic trace gases is to use Differential Optical Absorption Spectroscopy [Platt and Stutz \[2008\]](#). DOAS exploit the wavelength dependency of the absorption of light. Here the gas emissions can be retrieved from the quotient of the absorption signal of the volcanic plume and a reference region. This will be explained in a further chapter.

The reference region, is usually treated as free of volcanic trace gases. If the reference region is for any reason contaminated by volcanic trace gases, the reference spectrum has to be replaced by a volcanic-gas-free reference. Alternative spectra could be for example a theoretical solar atlas spectrum or a volcanic-gas-free reference spectrum recorded in the temporal proximity(eg. a day before) by the same instrument. The first option comes with the drawback of reduced precision, as the instrumental effects have to be modeled and added to the retrieval. The reduction in precision is acceptable for the SO₂ retrieval, but not suitable for a BrO retrieval because then most data would be below the detection limit. For the second option, the alternative reference spectrum should have been recorded at similar conditions with respect to meteorology and radiation as well as in the temporal proximity due to instrumental changes with time and ambient conditions. We combined both options in order to achieve both, enhanced accuracy but still maximum possible precision of the SO₂ and BrO retrievals. We present an algorithm which finds the optimal reference spectrum automatically. As first step, a possible SO₂ contamination of the standard reference is checked by a comparison with the theoretical solar atlas. If a contamination is detected, as second step, the algorithm picks a volcanic-gas-free reference (beforehand automatically checked for contamination) from another scan.

In this work we are mainly dealing with data from Tungurahua in Ecuador in the timespan of 01.08.2008 to 30.07.2009. Later on, we will also show the results of Nevado del Ruiz a volcano located in Colombia.

Part I

Theoretical Background

1.1 Volcanism and volcanic chemistry

volcano, n.: 1. Physical Geogr. A hill, mountain, or other feature, typically conical in form, that is built up of solidified lava and rock debris and has a crater or vent through which, in periods of activity, molten rock (lava), rock fragments, steam, and gas are emitted from within the planet's crust Oxford English Dictionary (2013) This chapter starts with a brief introduction to the reasons for volcanism and explains the different types of volcanism. Its purpose is to provide an overview of the complex processes happening during the long journey from the mantle and crust inside the Earth to the point at which the gases can be measured in the atmosphere. From melting rock and the magma degassing to the chemistry happening in the atmosphere, there are numerous processes influencing the amounts of gas and composition that are ultimately measured. The basics of volcanism described in Section 2.1 mainly follow the textbooks by Schmincke (2003), Francis and Oppenheimer (2004) and Frisch and Meschede (2013). The basic concepts of volatile degassing from the magma and which processes influence the chemical composition of the gases will be explained in Section 2.2. The chemistry of sulphur and bromine after their release into the atmosphere as well as the implications of volcanic degassing on the atmosphere and the Earth's climate will be discussed in Section 2.3. The introductory chapter will conclude in Section 2.4 with examples of the usefulness of volcanic gas emission measurements. An outlook will be given as to how measurements of the SO₂ emission rate and the chemical composition can be used to gain knowledge about volcanic systems and especially how they can help to improve the accuracy of volcanic eruption forecasts. 7

1.1.1 Volcanism

Volcanoes are the manifestation of large amounts of thermal energy inside Earth. A simplified depiction of the structure of Earth can be seen in Figure 2.1. Heat from the earth's core is to a large extent caused by decay of long-lived radioactive isotopes but also remaining from potential energy released by an increasing gravitational pressure during the formation of Earth. A small part might be caused by the impact of cosmic matter that collided with the Earth over the 4.5 billion years since the Earth's formation. A fraction the kinetic energy from these impacts is still stored in the core to this day (Francis and Oppenheimer, 2004). The transfer of heat from the Earth's core towards the surface can occur in different ways: conduction (which is not of importance in the context of volcanology), convection or mantle plume volcanism. Convection in the lower and upper mantle leads to movement of the oceanic and continental plates (also called lithosphere). At the margins of the lithospheric plates, increased volcanic activity occurs. In the case of constructive margins (i.e., new crust is formed) this phenomenon is called mid-ocean ridge volcanism for oceanic plates or continental rift zone volcanism for continental plates. In the case of destructive plate margins (i.e., the plate or slab sinks back into the mantle region) it is called subduction zone volcanism. A third, but less frequent,

path of heat transfer results from basaltic magmas that rise through a plume to the surface. This process leads to volcanism further away from plate margins, so called hot-spot volcanoes (e.g. the Hawaiian islands or Iceland). The geological setting influences the magma composition and gas content and therefore the shape and eruption style of a volcano. The evolution of magma from the point at which the rock melts to the time of an eruption influences the composition of the magma and - the most important aspect for this work - also the composition of gases released from volcanoes. The processes involved in the formation of mid-ocean ridge volcanoes, subduction zone volcanoes and hot-spot volcanoes are shown in Figure 2.1 and briefly summarised below:

- Mid-ocean ridge volcanism occurs when two oceanic plates are pulled apart, e.g. by the sides of a plate that sinks under another plate (see below, subduction zone volcanoes). The spreading of the plates leads to a thinned oceanic lithosphere. As a result of the thinner lithosphere, material from the upper mantle that is solid at depths lower than 100 km ascends to shallower depths of approximately 50 km. At this depth, the pressure is low enough for the mantle material to start melting. This type of volcanism leads to basaltic magma (low SiO₂ content, relatively few volatiles and low viscosity) that rises further and replenishes the gap between the two plates.
- Continental rift zone volcanism is in a way similar to mid-ocean ridge volcanism. The process leading to volcanism in this case is a continental plate that splits into two diverging plates. One important example of continental rift zone volcanism is the Nyiragongo volcano in the Democratic Republic of Congo.
- Subduction zone volcanoes are caused by an oceanic plate converging under another oceanic or continental plate. This type of volcanism is, for example responsible for the Andes. Two of the volcanoes that were examined during this thesis, Popocatépetl in Mexico and Nevado del Ruiz in Colombia, are subduction zone volcanoes. The descending plate is dense enough to sink back into the lower mantle and contains many water-rich minerals and sediments. During the descent the temperature of the plate increases due to an uptake of heat from the surrounding warmer mantle material and frictional heating. At a depth of several hundred kilometres, the plate will reach a temperature at which it starts melting and consolidates with the mantle again. Beginning at an earlier stage of approximately 80 – 150 km, water from the water-rich descending plate evaporates and rises into above the descending slab causes it to melt. The result of the melting process is water-rich magma with more volatiles than magma from midocean ridge volcanoes. Most of the magma at subduction zone volcanoes consists mainly of andesite, but since it can consist of melt from various parts of the earth (subducting plate, the upper mantle and continental lithosphere) basaltic, dacite and rhyolite magmas can be found as well. The low viscosity magma at subduction zone volcanoes is one of the causes for the violent eruptions.
- Hot-spot volcanoes can occur in the middle of oceanic or continental plates. They are a rare manifestation (only 5 include such important volcanoes as the Hawaiian islands, Yellowstone or Iceland. This type of volcano emerges when a hot spot at the coremantle boundary inside Earth leads to a plume in the mantle, a pathway in which solid material rises. When the solid material reaches approximately 100 – 150 km depth it partially starts to melt and

creates basaltic magma. During the further ascent the magma can interact with, e.g. continental crust, which in turn leads to rhyolitic, more-viscous magma. In some cases the solid material from the lower mantle consists of recycled lithospheric plates, which leads to a more complex magma. After magma is formed from molten rock, it can ascend further depending on its buoyancy. At some depth the concentration of dissolved volatiles exceed the solubility in the magma and a gas phase is formed. This might lead to degassing from the volcano. 10

1.1.2 Volcanic degassing

Volcanoes emit large quantities of various gases during eruptions but also during phases characterized by quiescent degassing. Emissions of volcanic gases into the atmosphere can influence the climate and serve as a precursor of volcanic activity. Even more, in most cases the exsolution of volatiles from the magma is the driving force behind the volcanic eruption. This demonstrates the importance of studying volcanic gas emissions. When measuring volcanic gas emissions it is crucial to understand the origin of the gas in order to find meaningful interpretations of the results. It is necessary to understand how gases are exsolved from the magma, how they are transported to the surface and which interactions during gas ascent can alter the gas composition. A simple model based on Henry's law can be used to explain degassing of volatiles from magma and the variability in the gas composition. Henry's law describes which equilibrium concentration c of a gas can be dissolved in a liquid with a Henry's constant k at a gas pressure p : $c = k \cdot p$ (2.1) In this model the melt starts at depth in a single liquid phase. As the magma rises the pressures decreases while c stays constant. When a volatile reaches saturation (i.e. $c > k \cdot p$) a second gas phase forms in addition to the liquid melt. This process is referred to as first boiling. The Henry's constant and thus the solubility of a volatile in the melt depend on the system's temperature as well as on the chemical composition of the liquid and the volatile. Another process called second boiling is caused by crystallization in magma that cools down. As most crystals contain almost no volatiles, the crystallization process leads to an increased concentration of volatiles in the melt, and can lead to degassing without changes of the system's pressure. This model can help explain the importance of measuring the ratio between different trace gases. Figure 2.2 shows an example of degassing due to Henry's law. Figure 2.2 (a) shows the vesicularity¹ of a melt as a function of depth. The vesicularity is shown for different starting concentrations of CO₂ and for three values of the CO₂/H₂O ratio. Higher CO₂ concentrations lead to exsolution of gas at greater depth, as does a higher CO₂/H₂O ratio. A magma with a start concentration of 1000 mg CO₂ per kg melt and a CO₂/H₂O ratio of 5 has a vesicularity of 50 all CO₂ and 70 the SO₂ and almost none of the HCl are exsolved. When ascending further the degassing of HCl will start at a depth of 100m while at this depth most of the H₂O has already exsolved. The composition of gases can therefore evolve, and in this example the SO₂/HCl ratio would decrease during magma ascent. Using this model gas compositions can give insights into processes at depth and the equilibrium

temperatures at which the gas phase was formed as long as the gas phase remains unchanged during ascent (Edmonds, 2008). In reality, however, exsolved gas bubbles need to rise to the surface to be observed. The rise of gas to the surface can alter the chemical composition and lead to patterns in the observed gas emission rates. While the mechanisms and how they can lead to degassing patterns will be described below, it is first necessary to address how the rise of gas can lead to variations in the chemical composition: Temperature changes of the ascending gas can lead to a re-equilibration (i.e., SO₂ reacts to H₂S at decreasing temperatures) and gases can also interact with crustal rock or groundwater during ascending. According to Giggenbach (1996) the composition of gases due to processes at depth does not vary during “conventional observational periods”. The author claims that most variations observed are not caused by variations of the magma at depth but due to processes during the ascent of the gases. However, these processes and therefore also the gas composition might still vary with volcanic activity. After gas bubbles are formed they need to ascend for degassing at the surface to occur. Two different models are frequently used to describe the behaviour of gas bubbles after their formation: the rise speed dependent (RSD) model and the collapsing foam (CF) model (Parfitt, 2004). In the RSD model bubbles form during magma ascent. As gas bubbles always have a lower density than the magma they are buoyant. Depending on the magma rise speed and the viscosity of the magma, the RSD model can explain two mechanisms for degassing. In a low-viscosity magma that ascends with a low velocity, the gas phase can form bubbles that can rise to the surface separately from the magma. This is called open-system degassing. During their ascent gas bubbles can also coalesce and form larger bubbles that rise faster. If the gas phase can leave the magma, the viscosity of the magma decreases, which in turn slows down the ascent. In magmas with higher viscosity and a relatively high rise speed the bubbles might not be able to coalesce but grow by diffusion and decompression. Gas bubbles cannot separate from the magma, but ascend together with the magma until it is erupted. This process is called closed-system degassing. The formation of a gas phase that rises together with the magma decreases the magmas density and can thus be a trigger for a faster magma ascent. The RSD model can be used to explain periodicities in volcanic activity. A simple model with a one-dimensional volcanic conduit containing rising magma is explained in Sparks (2003a,b). In this system the magma can obtain the two different steady states described above, which can be summarized as:

- Slow-ascending magma, in which bubbles can coalesce and leave the magma and the viscosity increases.
- Fast-ascending magma, in which bubbles form but cannot coalesce and rise with together the magma. This leads to lower-density magma which accelerates even more.

Figure 2.3 shows the magma flow rate as a function of magma chamber pressure. Between A and B we have the steady state where gas can leave the magma (open-system degassing). If the pressure in the conduit increases further, caused by material originating from the magma chamber the flow rate increases. At point B, the magma rises too fast for bubbles to coalesce and the system jumps directly to state C (there is no steady solution between B and D). In this regime the magma rises too fast for bubbles to escape. The gas phase

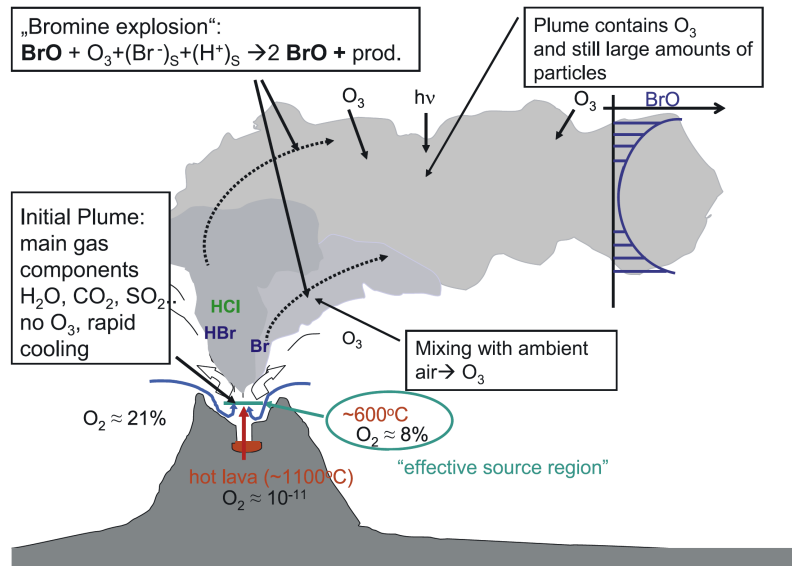


Figure 1.1:

leads to a lower density and this further accelerates the magma, which leads to an eruption of the system. In the eruptive state between point C and D material is transported out of the conduit faster than it is replenished from the magma chamber and the systems pressure decreases. The decreasing pressure and flow rate lead to point D. At point D the magma chamber pressure is too low to keep up the explosive regime, and with a further decreasing magma chamber pressure the system drops back to open-system degassing at point A. In the CF model magma is stored in a magma chamber or a dyke system at some depth (Parfitt, 2004). Bubbles form and rise to the top of the reservoir where they form a closely packed gas foam layer. Once the foam reaches a critical thickness, it collapses and forms a large gas bubble that rises up to the surface driving the volcanic eruption (Vergniolle, 1996). Depending on the viscosity of the magma either an annular flow (low viscosity) or a periodic series of gas slugs resulting from partial collapse of the foam (high viscosity) can be observed. The CF model can also explain periodicities in degassing patterns by the time needed to rebuild the foam layer to a critical thickness after its collapse. Magma does not necessarily need to erupt for degassing to occur. Degassed magma is more dense than volatile rich magma, and convection can lead to degassing, where the degassed magma sinks back into the magma chamber. This process can lead to substantial amounts of degassing without any erupted magma (Kazahaya et al., 1994; Stevenson and Blake, 1998). It is also often the case that more gas is released during an eruption than can be dissolved in the magma that was erupted. For example, during the 1982 eruption of El Chicón, Mexico, 40 times more gas was measured than was estimated from the erupted magma with petrological methods (Shinohara, 2008)

1.1.3 Volcanic gases and their impact on the climate

Volcanoes emit large amounts of gases into the atmosphere. In descending magnitude the most important gases are H₂O, CO₂, various sulphur species led by SO₂ and H₂S and halogen compounds (see Table 2.1). While water vapour is the most abundant gas in a volcanic plume, and responsible for the condensation of the plume that can be observed at many quietly degassing volcanoes from large distances, the total abundance is negligible when compared to evaporation from oceans. CO₂ emissions are thought to have played an important role during the formation of Earth's atmosphere. However, today CO₂ emission from volcanoes are several orders of magnitude smaller than anthropogenic CO₂ emissions. While anthropogenic CO₂ emissions were roughly 35 Gt (gigatons) in 2010, volcanic CO₂ emission estimates ranged between 0.13 - 0.44 Gt per year, comparable to the CO₂ emissions from countries as Pakistan (0.18Gt), Kazakhstan (0.25 Gt) or South Africa (0.44 Gt) (Gerlach, 2011, and references therein). However, on time scales of 105 a CO₂ degassing has an important role in the Earth system, since it offsets CO₂ burial in the sediments. SO₂ is the third most abundant gas and can be measured by remote sensing in the UV. It is therefore often measured as a proxy for volcanic activity. The yearly global SO₂ emissions by volcanoes range between 7.5 - 10.5TgSyr⁻¹ (Halmer et al., 2002) and are therefore of the same magnitude as anthropogenic SO₂ emissions (55TgSyr⁻¹ for the year 2000 were given in IPCC, 2013). SO₂ and BrO are the two trace gases in volcanic plumes that are the main topic of this thesis. This chapter therefore gives a brief overview over the chemistry of SO₂ and BrO in the atmosphere after emission from the volcanic vent. The impacts of volcanic gas emissions on the environment and especially the influence of SO₂ on the Earth's climate will be discussed following Robock (2000). The part about SO₂ summarizes parts of the review paper by Oppenheimer et al. (2011) and the chemistry of BrO is based on the papers of Bobrowski et al. (2007) and von Glasow (2010). Both parts also contain ideas from von Glasow et al. (2009). Regardless of the path of SO₂ scavenging, dry or wet deposition or oxidation to sulfuric acid, the molecule can influence the environment in several ways. A local effect, especially compared to the influences on the Earth's climate, are direct influences of SO₂ on humans (respiratory problems, asthma) and plants in the areas affected by volcanic gases. Acid rain caused by volcanic plumes can prevent the growth of plants. Darrall (1989) reviewed the influences of SO₂ on photosynthesis, and found that long-term exposures with SO₂ concentrations between 100 - 250 ppb can inhibit photosynthesis of plants. Delmelle et al. (2002) measured SO₂ concentrations around Masaya volcano, Nicaragua. The authors found concentrations of up to 230 ppb and an area downwind of the volcano with a decreased number of plant communities. Similar studies were done by Longo et al. (2005), who studied SO₂ concentrations and fine aerosol downwind of Kilauea volcano on Hawaii. The authors found high SO₂ concentrations of over 61.9 ppb with atmospheric sampling in the Kau desert south of Kilauea crater. Despite these lower SO₂ concentrations, plant growth is largely diminished in the Kau desert. Fig. 2.4 gives an impression of plants in the Kau desert. It should be noted,

though, that while SO₂ certainly has negative effects on plant life other species in the volcanic plume (e.g., HF) are most likely deposited within close proximity of SO₂ on the ground as well. Sulphur influences on the Earth's climate On a global scale, SO₂ and especially its oxidation product sulphuric acid have a large impact on Earth's climate. The total annual SO₂ emissions are low compared with anthropogenic emissions. Halmer et al. (2002) estimated mean annual S emitted as SO₂ by volcanoes between 1972 and 2000 to be in the range between 7.5 - 10.5TgSyr⁻¹. The estimates for anthropogenic SO₂ emissions for the year 2000 have a mean value of 55TgSyr⁻¹ (IPCC, 2013). However, Graf et al. (1997) suggested that the impact of volcanic SO₂ emissions is higher, since they are released into the free troposphere or into the stratosphere during eruptions, whereas most anthropogenic emissions are released into the planetary boundary layer. After emission into the atmosphere SO₂, is oxidised to sulphuric acid. The lifetime of sulphuric acid in the troposphere is only about 1 week compared with up to one year in the stratosphere (IPCC, 2013). Sulphuric acid directly influences the climate by backscattering radiation from the sun and thus increasing the Earth's albedo. Even more importantly it serves as additional cloud-condensation nuclei (CCN), which results in more and finer condensed particles and therefore in whiter, more-stable clouds and also an increased albedo of Earth (Twomey, 1974, and Fig. 2.5). This leads to more back-scattered radiation (see Fig. 2.5) and more diffusively scattered radiation. The net result of the back-scattered radiation is cooling of the Earth atmosphere, which is the dominating radiative effect of volcanic gases (Robock, 2000). Additionally, aerosol particles can also act as surfaces for heterogeneous reaction cycles that destroy ozone, especially in the stratosphere, which leads to an increased solar flux to the Earth. Larger aerosol particles can backscatter IR radiation emitted from the Earth's surface and the lower atmosphere and thus slightly reduce the net cooling effect in the lower troposphere. Absorption of direct UV and IR radiation from the sun as well as of radiation emitted by the Earth leads to net heating of the stratosphere. The 2013 IPCC report (IPCC, 2013) states that the radiative forcing caused by volcanoes was -0.11 Wm⁻² between the years 2008 and 2011 (for comparison, the radiative forcing of CO₂ was given as 1.68Wm⁻²). Another, counter-intuitive effect is the winter warming in the Northern Hemisphere, which is caused by changes of the stratospheric and tropospheric circulation patterns due to strong temperature gradients between the Arctic and equatorial regions (Robock, 2000).

1.1.4 Volcanic plume chemistry

1.1.5 Sulphur species

2.3.1 Sulphur species Sulphur species, mainly SO₂ and H₂S are the third most abundant species in volcanic plumes after H₂O and CO₂. SO₂ contributes up to 25volume of the volcanic plume and H₂S ranges between 1 - 10As opposed to the two most dominant species, SO₂ does not have considerable background levels in the atmosphere. The SO₂ concentration in the atmosphere is usually below 1 ppb

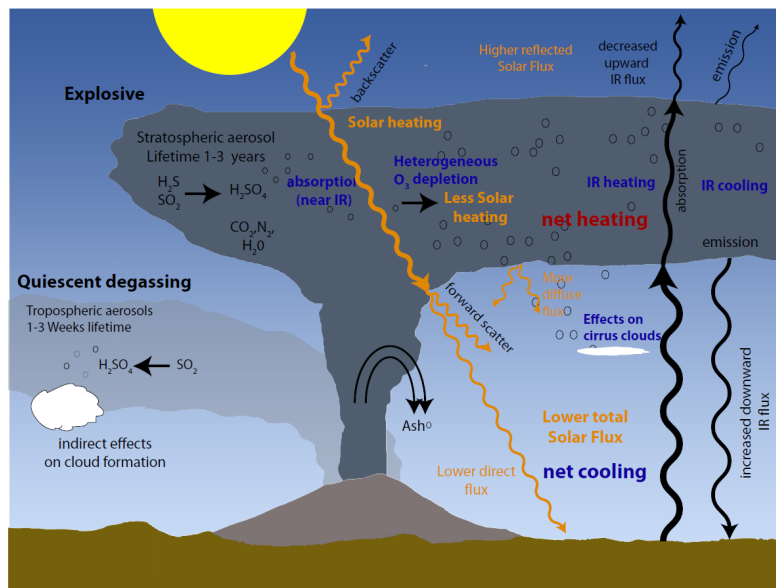


Figure 1.2:

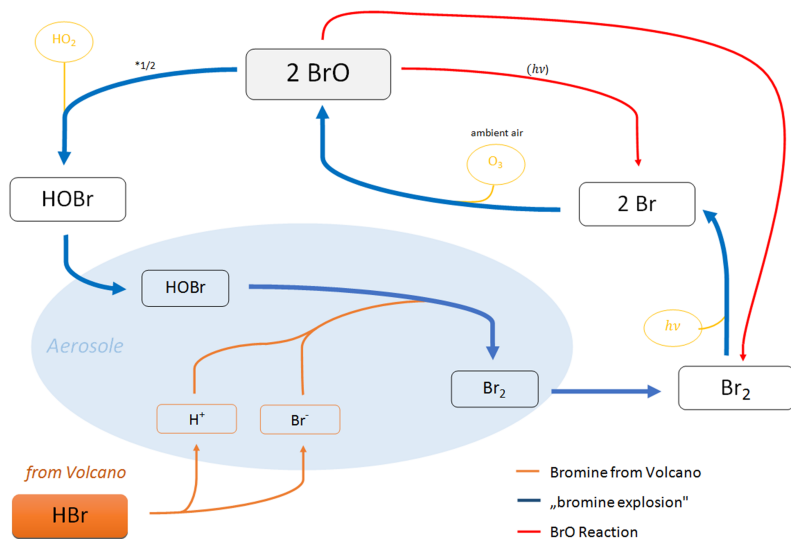


Figure 1.3:

while the concentration in a volcanic plume can easily achieve levels of 1 ppm (Oppenheimer, 2003a). The low background values together with the stability and the relatively strong UV absorption make SO₂ an easily accessible tracer for volcanic gas emissions (see next Section 2.4). After their release from the reducing conditions in the volcanic vent the gases enter the atmosphere, which is an oxidising environment. H₂S is slowly oxidized to SO₂ when released into the atmosphere. The first step is the reaction of SH. The SH radical then undergoes a series of reactions in the atmosphere that lead to the formation of SO₂ (Seinfeld and Pandis, 2006). Theoretically H₂S can react with the halogen radicals Cl and Br to form SH, which results in H₂S lifetimes of only a few seconds (Aiuppa et al., 2007). However, Aiuppa et al. (2007) could not reproduce these low H₂S lifetimes in measurements that showed a constant SO₂/H₂S ratio at distances up to several kilometres from the vent. SO₂ is removed from the atmosphere by wet and dry deposition or oxidized to sulphuric acid. In the gaseous phase the reaction with OH to sulphuric acid is rather slow: The rate constant k in Eq. C2.4 is given for 50 et al. (2004). Möller (1980) calculated an SO₂ loss rate of $k = 1.2 \cdot 10^{-6} \text{ s}^{-1}$ for homogeneous reactions in the gas phase, or converted to hours a loss of 0.43SO₂ per hour. In heterogeneous reactions, such as reactions of SO₂ on particles or in the liquid phase of particles, the oxidation process is much faster. Möller (1980) gave loss rates of $k = 0.1 - 1 \cdot 10^{-5} \text{ s}^{-1}$ for reactions of SO₂ on aerosol particles and $k = 5 \cdot 10^{-5} \text{ s}^{-1}$ for liquid phase oxidation. The equations for the reaction of SO₂ in the liquid phase are (Möller, 1980): SO₂ can be further oxidized to sulphuric acid or sulphate, e.g. by a reaction with OH (Platt and Stutz, 2008). The oxidation of SO₂ can also take place on aerosol particles by reactions with O₃, H₂O₂, HOCl, HOBr or oxygen if catalysts (iron, manganese) are available (von Glasow et al., 2009). Considering these different pathways and regarding the importance of SO₂ as a tracer for volcanic activity and for the comparison of SO₂ with other trace gases, it is worthwhile to compare measured SO₂ loss rates with the values given above. There are only a few reports of high SO₂ loss rates. Jaeschke et al. found $7 \cdot 10^{-4} \text{ s}^{-1}$, which would lead to an e-folding time between only 16 and 23 minutes. However, older data listed in Oppenheimer et al. (1998) showed times between 5 hours and several weeks. McGonigle et al. (2004) studied the depletion rate of SO₂ using the DOAS technique at Masaya volcano, Nicaragua. The authors found that there are negligible variations of up to 500 s - 2000 s after release from the volcano. Furthermore, the authors argue that Jaeschke et al. (1982) had problems with using CO₂ as a tracer to compare the SO₂ concentration. Meanwhile Oppenheimer et al. (1998) based the calculated loss rates on only a few traverse measurements, thus being influenced by variations in the total emission rate from the volcano as well as errors from wind speed and direction. Oppenheimer et al. (1998) measured ash plumes during the wet season at Soufriere Hills, Montserrat. Repeated measurements at the same volcano with more traverses during the dry season and ash-free volcanic plumes, found an one order of magnitude slower SO₂ loss rate (Rodríguez et al., 2008). Recent studies from satellites by Beirle et al. (2013) investigated the SO₂ loss rates at Kilauea, Hawaii. The authors found mean monthly SO₂ life times between 16 and 57 h, with the longer lifetimes in summer,

when the cloud coverage is lower. While satellites are not able to assess potential SO₂ loss close to the volcanic vent due to restrictions of their spatial and time resolution, this study still shows slow SO₂ loss rates with robust observations over a long time-scale. In this work it is assumed that SO₂ is stable during the time frame that usually occurs during ground-based remote sensing measurements (a few up to several tens of minutes during this thesis).

1.1.6 Bromine oxide

2.3.2 Bromine oxide Bromine oxide (BrO) was detected for the first time at Soufriere Hills volcano (Montserrat) by Bobrowski et al. (2003). Since then, BrO has been detected at many volcanoes by ground-based measurements (e.g., Bobrowski and Platt, 2007; Bobrowski et al., 2007; Oppenheimer et al., 2006; Vogel, 2011) or from airborne platforms (Heue et al., 2011; Kelly et al., 2013). Theys et al. (2009) were able to detect BrO from satellite after the Kasatochi eruption in 2008, and Hörmann et al. (2013) were able to find BrO in volcanic plumes from 11 erupting volcanoes with data from the GOME-2 instrument. However, it is actually mainly HBr, not BrO, that is emitted from volcanoes. BrO is formed after the volcanic gas mixes with ozone-rich ambient air. Gerlach (2004) and Martin et al. (2006) used thermodynamical equilibrium calculations to assess the source of bromine and found that there is not enough Br or BrO in hot magmatic gases to explain the BrO concentration measured, e.g. at Soufriere Hills by Bobrowski and Platt (2007). Instead, the volcanic gases mix with atmospheric air at high temperatures, in the so-called effective source region (Bobrowski et al., 2007), see Figure 2.6. This can be compared to a chimney, where hot air released from the volcano pulls in atmospheric air through the permeable edifice (Gerlach, 2004). The mixing process at high temperatures changes the gas composition and leads to an increase in bromine species other than HBr such as Br, Br₂ and BrO (Martin et al., 2006; von Glasow, 2010). Further mixing with atmospheric air leads to cooling down to ambient temperatures where the so-called Bromine Explosion starts. The term Bromine Explosion originates from BrO observations in polar regions, where a similar non-linear increase in BrO concentration has been observed (Hönninger and Platt, 2002; Lehrer et al., 1997; Wennberg, 1999). The Bromine Explosion mechanism can be summarized as: C2.8 and C2.9 describe the uptake of HBr and HOBr on the surface of an aerosol particle and subsequent transformation into the liquid phase. At low pH < 6.5 (Fickert et al., 1999) or at cold temperatures H+, Br- and HOBr react to form Br₂ (C 2.10) that is then released back into the gas phase (C 2.11). Br₂ reacts to Br via photolysis if sunlight is available (C 2.12). The necessity of solar radiation for the Bromine Explosion in volcanic plumes was verified by Kern et al. (2009), who could measure elevated BrO during daytime, but not at night at Masaya volcano, Nicaragua. In the next step Br that was formed from Br₂ and O₃ reacts to BrO (C 2.13). The role of O₃ in Eq.C2.13 was shown by Bobrowski et al. (2007) and Louban et al. (2009) who measured higher BrO/SO₂ ratios at the edges of the volcanic plume rather than in the middle of the plume, where less ambient (ozone-rich) air is available. Kelly et al.

(2013) was able to measure the evolution of ozone depletion in volcanic plumes from an airborne platform. BrO can react with HO₂ to form HOBr again leading back from C2.15 to C2.9. The result of this reaction cycle is the formation of BrO and the destruction of O₃. BrO can also react with another BrO molecule to form Br₂ or Br (C. 2.15 and 2.16), which in turn would react again to BrO. The Bromine Explosion reaction cycle is schematically shown in Figure 2.7. Considering the multitude of chemical reactions that take part in the formation of BrO and because BrO is a secondary volcanic gas, there is some discussion as to whether BrO/SO₂ ratio can be a useful indicator of volcano activity. If BrO/SO₂ ratios are used as an indicator of volcanic activity, influences from the formation of BrO in the atmosphere have to be ruled out or characterized carefully. SO₂ can be regarded as stable during times that are typically observed in ground-based remote sensing observations (see above). Perspectives on the time scales of BrO formation have changed over the last couple of years. Bobrowski et al. (2007) and Roberts et al. (2009) estimated an increase in the BrO/SO₂ ratio up to several tens of minutes after release from the vent. Newer publications and an improving dataset led Bobrowski and Giuffrida (2012) to the conclusion that the BrO/SO₂ ratio increases in the first minutes after release from the volcano, and then stays constant for some time (see Figure 2.8). Vogel (2011) and Gliß (2013) were able to measure the evolution of the BrO/SO₂ ratio in the young plume of Pacaya volcano and Etna volcano respectively using horizontal DOAS scanning measurements and found a strong increase within the first five minutes after release. Vogel (2011) also measured the BrO/SO₂ ratios in ageing plumes at Mt. Etna and found a constant ratio for plume ages of up to two hours. It has not been sufficiently examined if the BrO/SO₂ ratio depends on the ratio of Br/S exsolved from the magma. Nevertheless, it is important to rule out influences of atmospheric chemistry in order to find a meaningful interpretation of BrO/SO₂ ratios. The influence of the time following the mixing of volcanic gas with the ambient atmosphere will be discussed in Chapter 5.

1.1.7 Using volcanic gases to study volcanic activity

2.4 Using volcanic gases to study volcanic activity There are many factors influencing the degassing of volatiles and the composition of gases after and during the release from the volcanic vent. Furthermore the plume composition changes when it reacts with the oxidizing atmosphere. Therefore interpreting volcanic degassing data is complex. For example, Oppenheimer et al. (2011) reported in their review paper on SO₂ degassing, that decreasing SO₂ fluxes have been ascribed to:

- depletion of volatiles in a magma body
- decreased permeability of the magma in the conduit

The first process can be regarded as an indicator of decreasing volcanic activity. The second process can be caused by, for example, the formation of a plug when degassed magma starts crystallization. The plug leads to a build up of gas pressure and ultimately might lead to an eruption (Clarke, 2013). Therefore the observation of decreasing SO₂ emission rates can indicate an increase as well as a decrease of volcanic activity. Despite these complications, measurements of volcanic gases can

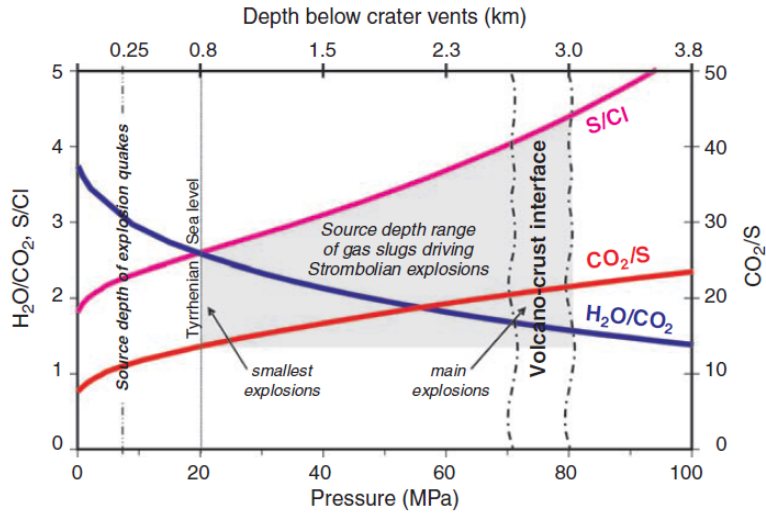


Figure 1.4:

be an important additional tool for the forecasting of volcanic activity to accompany the classic monitoring techniques like seismicity or deformation measurements. The remote sensing of volcanic gases started with the correlation spectrometer COSPEC (Moffat and Millan, 1971; Stoiber et al., 1983) in the 1970 s. COSPEC measurements together with fumarolic sampling helped, for instance, predict the eruptions of Mount St. Helens, USA, in August 1980 and June 1981 (Casadevall et al., 1983) or Pinatubo, Philippines, in 1991. The remote sensing of volcanic SO₂ experienced further spreading world-wide with the availability of miniature spectrometers (Galle et al., 2003) that measure the SO₂ column density by using Differential Optical Absorption Spectroscopy (DOAS, Platt and Stutz, 2008). Besides being smaller and cheaper, these miniature spectrometers using the DOAS technique have additional advantages for fieldwork in rugged environments, as they are lighter and consume less power. Additionally the availability of more spectral information allows for the correction of radiative transfer problems (Kern, 2009, and also Chapter 3) and to retrieve other trace gases (e.g. O₃, NO₂ or BrO). An important step towards continuous monitoring of volcanic SO₂ emission rates was made with the Network for Observation of Volcanic and Atmospheric Change (NOVAC, Galle et al., 2010). During this EU-funded project scanning DOAS instruments were installed at several volcanoes world-wide. The spectroscopic data for the BrO/SO₂ ratios evaluated within this thesis were recorded by the NOVAC network, which will be discussed in more detail in Chapter 5. Besides the monitoring instruments and the network itself, the detection of abnormally high SO₂ emission rates at Santa Ana volcano (El Salvador) before the eruption in 2005 was the first big success of the project (Olmos et al., 2007). These measurements helped to plan the evacuation of thousands of people living in the vicinity of Santa Ana volcano. Scanning DOAS instruments need approximately 5 – 15 minutes for one scan across the complete sky. These

techniques are therefore rather suited to measure long-term variations in the SO₂ emission rates. A lot of additional information can be gained when using instruments that allow emission rate measurements with a higher time resolution. Boichu et al. (2010) used two spectrometers with an optical system that led to a wide field-of-view covering the complete volcanic vent at Mount Erebus, Antarctica. This set-up allowed SO₂ emission rate measurements with a time resolution of the order of 1 Hz. Frequency analysis of the data revealed patterns with periods between 11 and 24 minutes that allowed discussion of different models for the degassing at Mt. Erebus. The SO₂ camera, which is also used in large parts of this thesis, makes SO₂ emission rate measurements with a similar time resolution possible. Holland et al. (2011) used SO₂ camera measurements at Santiaguito, Guatemala to identify shear-fracturing as the main process leading to cyclic patterns of explosive eruptions rather than building of a viscous plug. Tamburello et al. (2013) applied SO₂ cameras at Etna, Italy, using a similar approach as Boichu et al. (2010), and suggested that periodic signals with periods between 40 – 250 s and 500 – 1200 s are caused by bursting of rising gas bubbles. First steps in the direction of the analysis of high time resolution SO₂ camera data are presented in Chapter 4 of this thesis. In addition to the SO₂ emission rate, the ratio between different trace gases can be indicative of volcanic activity as well. The solubility of volatiles depends, e.g. on depth and chemical composition of the magma (see Chapter 2.1), therefore the composition of volcanic gases has been studied in depth. A good introduction to gas compositions and their interpretation can be found in Giggenbach (1996). A more recent review article about halogens in volcanic system was published by Aiuppa et al. (2009). Initial studies (e.g. Noguchi and Kamiya, 1963) investigated the Cl/S ratio by direct sampling. The authors found a decrease of the Cl/S ratio before an eruptive period (Noguchi and Kamiya, 1963; Stoiber and Rose, 1970). Later Pennisi and Le Cloarec (1998) found that Cl and F degas in a similar manner, while the Cl/S ratio varied between non-eruptive and eruptive periods. The authors argue that chlorine is exsolved from the magma at deeper levels (Cl/S > 1) while at shallower levels sulphur degassing dominates (Cl/S CO, SO₂ and HCl) by remote sensing using an open-path Fourier transform infrared spectrometer (OP-FTIR) at Stromboli, Italy. The authors found that the ratio of CO₂/SO₂ and SO₂/HCl were 3-5 times higher during explosions than during quiescent degassing. These observations paired with higher equilibrium temperatures lead the authors to the conclusion that the explosions are driven by gas slugs that originate from a deeper level than gas observed during quiescent periods. The authors then used melt inclusion data and a chemical model simulating degassing of magma to interpret the data. The S/Cl and H₂O/CO₂ ratios show that bigger explosions originate from a depth of approximately 2.7 – 3 km while smaller eruptions originate from depths as shallow as 0.8 km below the crater at sea level. The BrO/SO₂ ratio has been measured using DOAS remote sensing measurements by several authors (e.g., Bobrowski and Platt, 2007; Bobrowski et al., 2003, 2007; Hörmann et al., 2013; Kelly et al., 2013; Oppenheimer et al., 2006; Theys et al., 2009; Vogel, 2011). However, despite naming the possibility to use BrO/SO₂ ratios as an additional tracer for volcanic activity, most

of these studies focused on the formation of BrO in the atmosphere. First long-time measurements at Etna, Italy, were published by Bobrowski and Giuffrida (2012). The authors measured the BrO/SO₂ ratio covering the years 2005 - 2009 and found higher ratios during non-eruptive periods. During four eruptive periods BrO/SO₂ ratios were higher three months before the eruption compared to the ratios observed one month before the eruption. Studies on the seasonal variability and the influence of humidity did not reveal obvious correlations. The authors suggested a model in which bromine is released earlier than sulphur during the magma's ascent to explain the observed behaviour.

1.2 Remote sensing of volcanic gases

Remote sensing of volcanic gases In this thesis, SO₂ and BrO in volcanic plumes are measured with two different remote sensing techniques, Differential Optical Absorption Spectroscopy (DOAS, Platt and Stutz, 2008) and SO₂ camera. Both techniques make it possible to measure volcanic gases by examining their interaction with radiation. This chapter will briefly describe absorption and scattering of radiation in the atmosphere in Section 3.1. The concepts of the two measurement techniques will be described in Sections 3.2 and 3.3. The chapter concludes with the effects of radiative transfer on remote sensing measurements in Section 3.4.

1.2.1 Absorption spectroscopy

Beer-Lambert Law

Atoms and molecules exist in several energy states with varying electron configuration. Molecules can additionally have different rotational and vibrational states. For simplicity, the basics of radiation transport in the atmosphere will be explained only for molecules in the following paragraphs. If the energy of a photon matches the energy gap between two states of a molecule, the molecule can absorb the photon and enter the more energetic state. The transition can only occur if the lower energetic state is occupied and if the selection rules are fulfilled. The molecule can return to a lower state by collision with other molecules or emission of a photon. However, the direction of the emitted photon is usually not the direction of the incoming radiation. Therefore, the radiation intensity measured behind an absorbing medium (e.g. gases) decreases with increasing light-path through the medium. This decrease is described by the Beer-Lambert law. For radiation of wave- length and an initial intensity I_0 traversing a medium, the Beer-Lambert law gives the light intensity I after passing through a path of length L ,

where $c(l)$ is the location-dependent concentration of the trace gas of interest and is its absorption cross section. The absorption cross section is unique for each molecule and depends on pressure p as well as on temperature T . The quantity measured with many optical remote sensing techniques is the optical density ,

where S is the column density, the concentration of the trace gas integrated along the light-path:

The concentration c for a constant trace gas distribution can be directly calculated from the column density S if the path length L is known. For measurements in the atmosphere, the situation is more complex, with a multitude of different absorbers and scattering processes, such as Rayleigh scattering (see Section 3.1.2) and Mie scattering (see Section 3.1.2) that have to be taken into account. This is done by treating the scattering effects as pseudo-absorbers with their respective extinction coefficients R for Rayleigh scattering and M for Mie scattering. The extended Beer-Lambert Law reads:

This equation is valid for radiation traversing a medium of total length L , with several absorbing species j that can have variable concentrations c_j depending on the position l in the light path. The first two terms in the exponential function in Eq. 3.4 describe the extinction due to Rayleigh and Mie scattering in the atmosphere; the third term describes the absorption of various molecules. For simplicity, inelastic scattering and effects arising from turbulences in the atmosphere are neglected here. The most important effect of inelastic scattering, the Ring effect, will be described in Section 3.1.2 and 3.2.2.

1.2.2 Scattering processes in the atmosphere

Rayleigh scattering Rayleigh scattering describes elastic scattering (the photon energy does not change) on particles much smaller than the wavelength of the incident radiation. It has a strong wavelength dependency, scattering at shorter wavelengths is stronger, which leads to the blue colour of the sky. Platt and Stutz (2008) gave a simplified estimate of the Rayleigh scattering cross section:

Rayleigh scattering is (as the name implies) a scattering and not an absorption process. However, in the narrow-beam approximation it can be treated as an absorption process. This approximation assumes that the probability of a photon that was scattered out of the light beam is scattered back into the light beam is negligible. The Rayleigh extinction coefficient R for a number density of air molecules N_{air} is given by:

The angular distribution of Rayleigh-scattered photons is given by the Rayleigh phase function:

10 (3.7) Forward or backward scattering is stronger by up to a factor of 2, when compared to a scattering angle of $\theta = 90^\circ$. Scattering and absorption by particles Photons can also interact with particles that have a size comparable to the wavelength of the incident radiation (via scattering or absorption). For spherical particles this process is described by the Mie theory. Because these particles can absorb and scatter radiation, the Mie extinction coefficient is divided into two parts

with the particle radius r , the scattering coefficient s and the absorption coefficient a . Mie theory in general is very complex, even more for complex particle shapes. Therefore, only a few general remarks from Platt and Stutz (2008) will be given here. The single scattering albedo (SSA) of an aerosol is defined as:

It defines the amount of radiation scattered by Mie particles, compared to the amount that was scattered or absorbed. An SSA of 1 describes pure scattering, whereas an SSA of 0 describes an aerosol that absorbs all radiation. Mie scattering is, similar to Rayleigh scattering, not an absorption process; however, it can be described as an absorption process in the narrow-beam approximation as well. The wavelength dependency of the Mie extinction coefficient M is:

related to the size of the aerosol particles. In general, Mie scattering exhibits a smaller wavelength dependency than Rayleigh scattering. Spinetti and Buongiorno (2007) measured the optical properties of aerosols in the plume of Etna, Italy and found angstrom exponents between 0.13 and 2.42 during episodes of quiescent degassing. The Mie phase function, and thus the scattering direction, depends on the

(3.11) In general it can be said, that forward scattering is more dominant in Mie scattering when compared to Rayleigh scattering, especially for increasing values Raman scattering In addition to elastic scattering, inelastic Raman scattering (i.e. the energy of the photon changes during the scattering process) may also occur in the atmosphere if the atom/molecule changes its excitation state during the scattering process. The photon can transfer energy to the molecule (Stokes process) or take up energy from the molecule (anti-Stokes process). If only the rotational state of the molecule changes the process is called Rotational Raman scattering is used. When the vibrational excitation state changes as well, it is called rotationalvibrational Raman scattering. The cross sections for Raman scattering are orders of magnitudes smaller than those for Rayleigh scattering (Platt and Stutz, 2008). However, the influence of Raman scattering has to be considered for remote sensing applications. Due to the energy exchange during the scattering event, the incident photon has a different wavelength after the scattering process. This causes an effect known as the “Ring effect”, which is named after Grainger and Ring (1962). The Ring effect describes a decrease in the optical depth of the Fraunhofer lines due to photons that are inelastically scattered. The Ring effect is described in more detail in Section 3.2.2.

1.2.3 Differential Optical Absorption Spectroscopy(DOAS)

Eq. 3.4 cannot be applied to real measurements because obtaining the background intensity I_0 without absorbers would require removing the atmosphere. Additionally it is impossible to distinguish between the various broad-band effects, like scattering in the atmosphere or instrumental factors that influence the measured spectra. Differential Optical Absorption Spectroscopy (DOAS) is a technique that was invented in the late 1970s by Perner and Platt (1979) and that overcomes these drawbacks by using only the narrow-band absorption features of molecules to measure their column densities. This chapter will give a brief overview of the basic concepts applied in this thesis. More detailed information can be found in the comprehensive work by Platt and Stutz (2008), which was the foundation for this section. 3.2.1 The DOAS principle The DOAS technique takes advantage of the fact that scat-

tering effects as well as instrumental properties (i.e. the wavelength dependency of the spectrometer's optical system and grating) have a broad-band structure. The absorption cross section of trace gases on the other hand has spectral broad-band as well as narrow-band features. It can be divided into the following two parts: a broadband part that only varies weakly with wavelength and a narrow-band part which varies strongly with wavelength:

The Beer-Lambert law (Eq. 3.4) can now be rewritten with the exponential function separated into one part that contains all broad-band effects (e.g., scattering as well as broad-band absorption features) and another part that only contains the narrow-band absorption features of the trace gases:

The newly defined intensity I_0 is the intensity without differential absorption, it differs from I_0 only in broad-band structures. Using I_0 , the differential optical density can be defined (note that in this equation the differential absorption cross sections s_j are used, see also Fig. 3.1):

Eq. 3.14 can now be solved for the column densities s_j . For the simple case of only one trace gas with constant concentration c and a well-known light path L , the concentration can be directly calculated from

(3.15) In a DOAS measurement only the difference of the column density S_M in the measurement spectrum and the column density S_R of the reference spectrum is obtained. The optical density is given by:

In general for two spectra the obtained column density is called differential slant column density dS . In the case that the reference reference spectrum IR does not contain the trace gas of interest ($S_R = 0$) it is called the slant column density (SCD), the column density along some light path. In volcanological setting the ideal light-path is a straight line through the volcanic plume. In this thesis, it is usually assumed that the reference spectrum is gas free. Whenever the term column density is used it refers to the SCD. Only in Chapter 8 the distinction between dS and the SCD is explicitly made. 3.2.2 Technical implementation of the DOAS approach The theory described above is based on an ideal instrument. In reality, instruments have limitations; spectrometers only have a finite optical and spectral resolution and temperature dependencies can further influence the signal. The chapter above also neglects the effect of inelastic scattering that causes the Ring effect and also the solar I_0 effect, an effect that influences the convolution of the high-resolution reference cross sections. All these effects will be described in this section. The section ends with a brief description of the DOASIS software's fitting routine (Kraus, 2006), which was used for the evaluation of spectroscopic data in this thesis. Optical and spectral resolution of the spectrometer The optical and spectral resolution of spectrometers is finite. This leads to a spectrum arriving at the detector that can be described as the convolution of the incident spectrum with the instrument line function (ILF) :

To correctly retrieve the column densities s_j , all reference cross sections j used in Eq. 3.15 must have the same spectral resolution as the instrument used for recording the spectra. This can be achieved, for example, by recording absorption spectra and placing a calibration cell containing a known concentration of the trace gas of interest

in the light path. However, this is difficult to achieve in many cases. Some species are too chemically reactive (e.g. the equilibrium between NO₂ and N₂O₄ depends on the temperature) and additionally calibration cells tend to leak. For O₃, the temperature dependency of the absorption cross section presents another problem. Therefore, cross sections at instrument resolution are often calculated from high-resolution absorption cross sections measured in a laboratory by convolving them with the ILF H():

In DOASIS, the convolved spectrum is interpolated to the spectral grid of the spectrometer after the convolution. Equation 3.18 is only an approximation that can be used for small optical densities. A more accurate solution is shown in the subsection about the solar I₀ effect. The ILF H that is needed for the convolution can be approximated by measuring the lines of a Mercury lamp. The spectral width of these lines is typically only a few pm. Therefore, these lines can be seen as a delta peak in good approximation when compared to the resolution of a typical spectrometer (on the order of 0.6nm for the instruments used in this thesis). Effects from the detector The spectrum is recorded by a detector that only has discrete pixels. Therefore, a wavelength-interval is mapped onto a pixel i: $I_0(i) =$

For the DOAS retrieval, it is important to know the relationship between the channels of the detector and the wavelength of the spectrum. The so-called wavelength-pixel-mapping for a detector with q channels can be described with a polynomial:

The parameters k describe which wavelength corresponds to which pixel. 0 corresponds to a shift of the spectrum, and a change in 1 describes a squeeze or stretch of the spectrum. The wavelength-pixel-mapping as well as the optical properties of the spectrometer depend on the instrument's temperature and the ambient pressure in many cases. The temperature dependency is discussed in more detail in Chapter 7. To determine the wavelength-pixel-mapping, the peaks of a Mercury line spectrum are measured in many applications. From the known wavelength of the peaks and the pixels that correspond to these peaks the wavelength-pixelmapping can be determined. More recently the wavelength-pixel-mapping is determined by comparing a high-resolution solar spectrum (Chance and Kurucz, 2010), which is convolved to the instrument's resolution with the measured spectrum (Lehmann, 2014; van Rozendaal, 2013). The latter approach is used in this thesis, as Mercury line spectra for the NOVAC instruments were only available at room temperature. Two other important temperature-dependent effects of the detector are offset and dark current. The offset is a low voltage that is added to the CCD signal to prevent negative signals that could result from noise at very low intensities. The analog-to-digital converter that converts the signal to a digital value cannot handle negative values. The offset structure is temperature dependent and each instrument has an individual offset structure. It can be removed by subtracting an offset spectrum, which can be created by recording n spectra with minimal exposure time and no radiation entering the spectrometer. The offset spectrum has to be rescaled to match the number of spectra summed up in the measurement spectrum. The dark current of the CCD is caused by thermally excited electrons in the semiconductor's depletion zone. The dark current signal increases linearly with increasing exposure times

and exponentially with increasing temperatures and can be greatly reduced by cooling the detector. Additionally, it is signal dependent (Stutz and Platt, 1993), but a first-order correction can be made by subtracting a dark current spectrum from the offset-corrected measurement spectrum. The dark current spectrum should be recorded at the same temperature as the measurements, with no radiation entering the spectrometer and an exposure time longer than the measurement's exposure time. It has to be rescaled to match the measurements exposure time. The complete process of how radiation is measured and the incident spectrum is altered by the instrument's optical system and subsequently mapped onto discrete channels recorded by the detector is depicted in Figure 3.2. The Ring effect Inelastic scattering leads to the Ring effect (named after Grainger and Ring, 1962) that can be observed as a filling of the Fraunhofer lines in spectra of scattered solar radiation when compared to direct sunlight measurements. Today, it is believed that the Ring effect is caused by rotational Raman scattering mainly on O₂ and N₂ in the atmosphere (Bussemer, 1993; Solomon et al., 1987). Solomon et al. (1987) suggested treating the Ring effect as a pseudo-absorber in the evaluation of spectroscopic data based on the calculation listed below. The radiation arriving at the instrument I_{meas} consists of parts that were Rayleigh, Mie or Raman scattered in the atmosphere: $I_{\text{meas}} = I_{\text{Rayleigh}} + I_{\text{Mie}} + I_{\text{Raman}} = I_{\text{elastic}} + I_{\text{Raman}}$ (3.21) The logarithm of I_{meas} can be expanded when taking into account that Raman scattering is orders of magnitude weaker than elastic scattering processes:

The Ring spectrum that can be included as a pseudo-absorber in the DOAS evaluation is defined as: $I_{\text{Ring}} = I_{\text{Raman}} / I_{\text{elastic}}$ (3.23) The Raman Spectrum is needed for the calculation of the Ring effect. It can be measured by comparing the intensities of light that is polarized perpendicular and parallel to the scattering plane (Bussemer, 1993; Solomon et al., 1987). Another approach is to calculate the Raman spectrum from a measured spectrum using input knowledge on the concentrations of N₂ and O₂ in the atmosphere (Bussemer, 1993; Chance and Spurr, 1997). In this thesis, the latter approach is used with the Ring spectrum being calculated from the DOASIS software package (Kraus, 2006). In cases with multiple Rayleigh scattering in the atmosphere or scattering on clouds and aerosol particles, the wavelength dependency of the amplitude of the Ring spectrum can vary (Wagner et al., 2009). For these cases a second Ring spectrum, which is calculated from the original Ring spectrum by multiplying it by a wavelength dependent term α , is included in the evaluation: $I_{\text{Ring},2} = I_{\text{Ring}} \alpha$ In this work, the second Ring spectrum is orthogonalised against the first Ring spectrum in the retrieval range. The solar I₀ effect As outlined earlier in this section, typical spectrometers have a finite resolution that cannot resolve all the structures of the Fraunhofer lines. The absorption structures as seen by the spectrometer can therefore differ slightly from the absorption cross sections that were recorded in the laboratory with an unstructured light source and later convolved to match the instrument's resolution (Platt et al., 1997). Two effects called the solar I₀-effect and the saturation effect can occur. Both effects are caused by narrow spectral structures that are not accurately taken into account when using cross sections as outlined in Eq. 3.18. For the saturation effect, these are strong

absorption lines that are smoothed out during the convolution of the cross section. For the solar I0-effect, the causes are narrow Fraunhofer lines that weight a cross section differently in reality. Mathematically this can be shown by comparing an ideal measurement (infinite resolution) with one trace gas with a real measurement. For an ideal measurement, the DOAS approach would yield the optical density:

In reality, however, both intensities are measured with the instrument's spectral resolution (see Eq. 3.17) and the optical density is:

Therefore, for strong absorbers or a structured light source (as the sun in passive DOAS measurements), a correction has to be applied. Following Platt and Stutz (2008) and Lehmann (2014), the corrected absorption cross sections 3 Remote sensing of volcanic gases can be calculated as:

In this equation 0,K is calculated by convolving a high resolution solar spectrum (e.g. Chance and Kurucz, 2010):

For the second spectrum K an absorbing term according to Beer-Lambert law is applied before the convolution:

A good estimate of the true column density is therefore needed to create the corrected absorption cross sections. In this work, whenever solar I0-corrected cross sections are used, the estimate was obtained by performing a fit using cross sections according to Eq. 3.18. The obtained column densities were then used as input parameters for Eq. 3.27. The DOAS retrieval The DOAS approach used in this thesis differs slightly from Eq. 3.14 and 3.15. The fitting routine from the DOASIS software (Kraus, 2006) was used to evaluate all spectroscopic data in this thesis. Eq. 3.4 can be rewritten to:

differ between the background spectrum I0 and the measurement spectrum I. The DOAS fitting routine varies the polynomial and the column densities

The DOASIS fit routine uses a combination of a standard least-squares fit and a Levenberg-Marquard algorithm to minimize

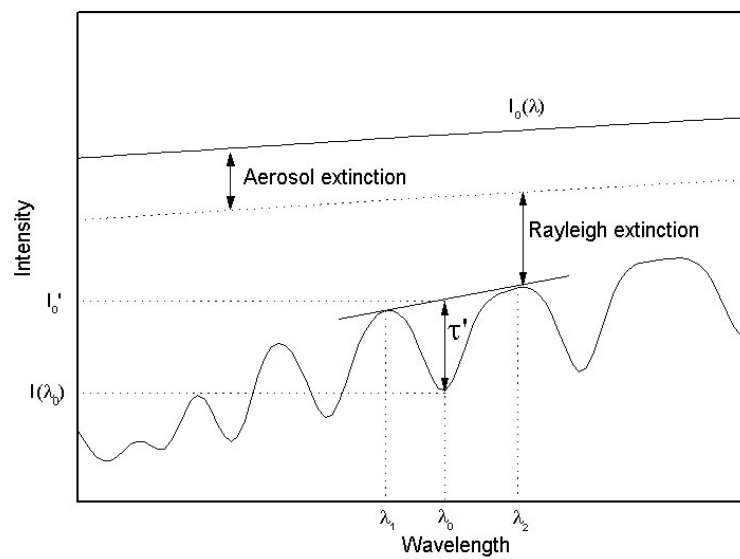


Figure 1.5:

Part II

Evaluation of the Data of Tungurahua and Nevado Del Ruiz

2 Network for Observation of Volcanic and Atmospheric Change

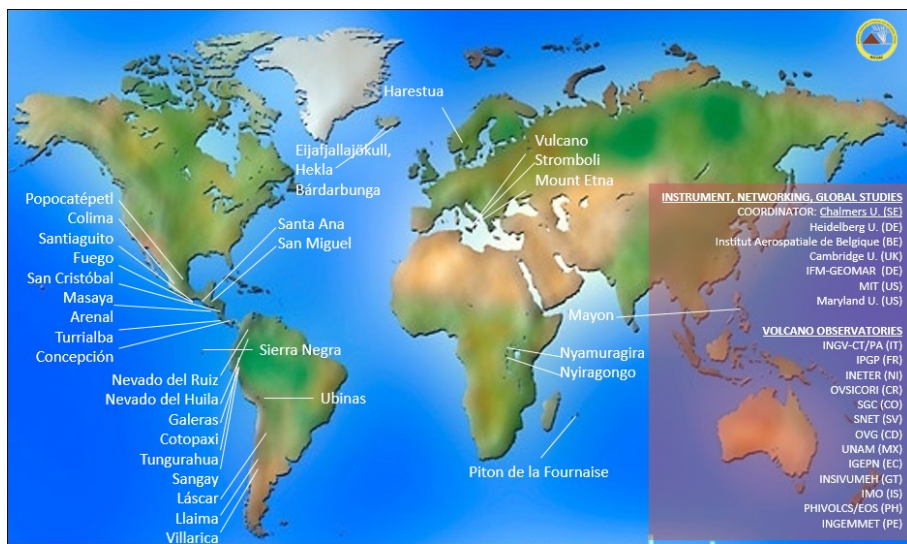


Figure 2.1: Global map of the volcanoes monitored by NOVAC. Used with friendly permission of Santiago Arellano.

Network for Observation of Volcanic and Atmospheric Change (NOVAC) is a network of instruments monitoring volcanoes over the hole world. The aim of NOVAC is to gain another tool for risk assessment, for gas emissions and geophysical researches. Also many other scientific purposes are build on the data from NOVAC. Figure 2.1 shows a map, with all volcanoes of the Network for Obersavation of Volcanic and Atmospheric Change.

NOVAC was originally funded by the European Union on the first October in 2005. The aim of NOVAC is to establish a global network of stations for the quantitative measurement of volcanic gas emissions. At the beginning NOVAC encompassed observatories of 15 volcanoes in Africa America and Europe, including some of the most active and strongest degassing volcanoes in the world. Although the EU-funding has stopped, the network has been constantly growing since it was founded. In 2017 more than 80 Instruments are installed at over 30 volcanoes in more than 13 countries.

The great advantage of the data monitored in NOVAC is the fact that NOVAC provides continues gas emission data over many years. Therefore one is able to get more statistical stable results.

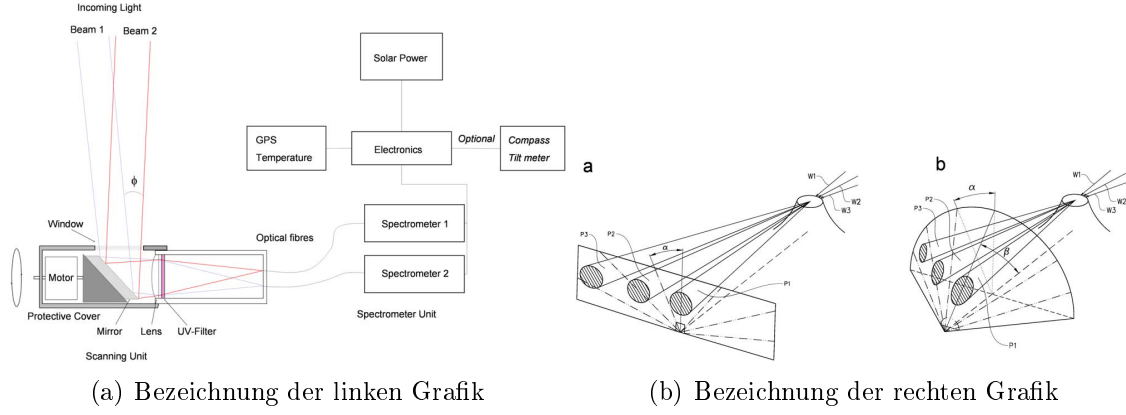


Figure 2.2: Titel unterm gesamten Bild

The instruments used in NOVAC are scanning UV-spectrometer : Mini Doas instruments.

The Mini-DOAS instrument represents a major breakthrough in volcanic gas monitoring as it is capable of real-time semi-continuous unattended measurement of the total emission fluxes of SO₂ and BrO from a volcano. Semi-continues means in this case that the measurement is only possible during day time when enough Sun light is there.

The basic mini-DOAS system consists of a pointing telescope fiber-coupled to a spectrograph. Ultraviolet light from the sun, scattered from aerosols and molecules in the atmosphere, is collected by means of a telescope with a quartz lens defining a field-of-view of 12 mrad. ??

The spectrometers measure in the UV region in a wavelength range of 280 to 420 nm. In this range are the differential structures of SO₂ and BrO dominant.

The Novac-instruments need to be very robust to stand the conditions around volcanoes. Therefore the design of the instruments is rather simple, this means the instruments do not have internal stabilisation features like temperature stabilization to keep the measurement independent of external parameters (for example Temperature). This comes along with a reduced precision of the data, but the huge amount of data produced by NOVAC compensates this disadvantage.

2.1 Measurement Routine

The Instruments are set up five to ten km downwind of the volcano of the volcano. To cover most of the occurring wind directions two to five instruments are installed at each volcano. Ideally the measurement plane is orthogonal to the plume, to get the best measurement results. In reality the measurement plane could be twisted. The Instruments record spectra in different viewing angles covering a the hole sky from horizon to horizon from -90° to 90°. The zenith is at 0°. The measurement routine starts with a spectrum in zenith direction: The pre-reference. Afterwards

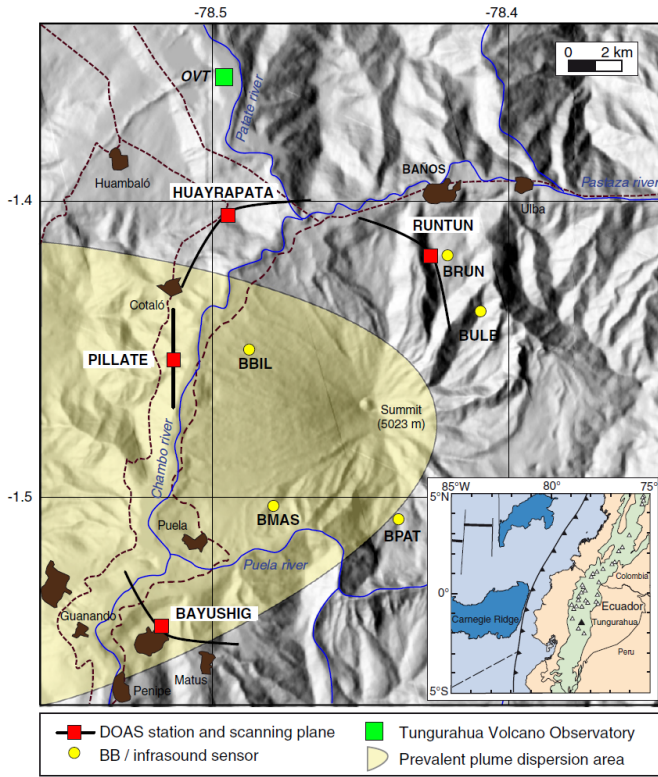


Figure 2.3:

the dark current spectrum is recorded.

Then the Instrument turns automatically to the side, recording spectra at the Elevation Angle from -90° to 90° with steps of 3.6° .

One hole measurement takes from 6 to 15 minutes.

3 Evaluation Routine

3.1 NOVAC-Evaluation

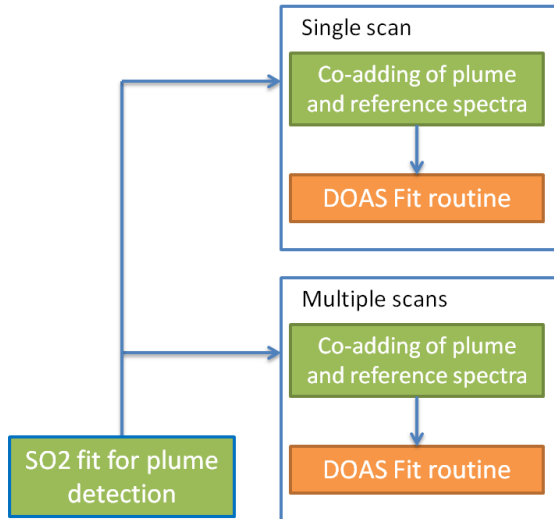
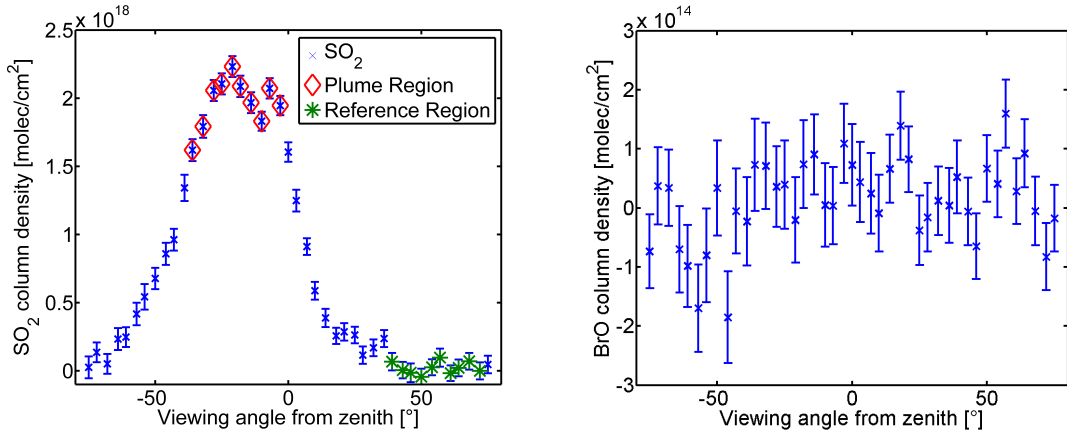


Figure 3.1:

In the following we describe the technical implementation of the DOAS approach using the data of NOVAC instruments:

The first important task is to locate volcano plume and the reference region using the data from the measurement routine described above.

To do so we use the pre-reference (the spectra recorded at an elevation angle of 0°) to evaluate spectra for SO₂ at every elevation angle as described in chapter 1.2.3, that means we divide each recorded spectra by the pre-reference and take the logarithm to get rid of the Fraunhofer structures and to be able to just look at the important structures of the plume. To get the gas amounts of the evaluated spectra, one fits the absorption spectrum of all important gases on the spectrum. In our case we take all gases written in tab. ?? into account. The result will be an SO₂ curve as it is shown in fig. ???. Figure ?? shows the relative SO₂ column density to the pre-reference as a function of the elevation angle. We can clearly observe a maximum of SO₂ and a minimum. Inside the plume the SO₂ amount is much higher than in the outside the plume. Therefore we assume that the location of the SO₂ maximum matches with the location of the plume. We assume that the minimum of the SO₂ curve refers to a region outside of the plume which is in most



(a) Bezeichnung der linken Grafik

(b) Bezeichnung der rechten Grafik

Figure 3.2: Titel unterm gesamten Bild

times the case. The SO₂ amount in the earths atmosphere is negligible so we take it as a region of zero SO₂. Now it is possible to locate the plume region as the SO₂ maximum, whereas the minimum of the SO₂ curve the reference region is.

To technically detect the plume region we use a gauss fit of the SO₂ curve. To increase the quality and to get a more robust result the sum over several plume spectra is taken. If the gauss curve is too wide we use only the 10 spectra with the highest SO₂ amount. For the reference we use the sum of 10 spectra with the lowest SO₂ amount.

The so found reference spectrum is used to fit it on the SO₂ absorption lines of Gases to get the absolute column densities of SO₂ and BrO in the plume spectrum

Since the BrO column density is much lower than the SO₂ column density and lies just slightly above the detection limit the plume is hard to detect using the BrO column density as it is shown in fig. ???. Therefore we use plume location we found by using SO₂ to evaluate the BrO column density.

For the evaluation we use the data of more than one measurement, to increase the fit quality.

We are mainly interested in the BrO/SO₂ ratio, with the calculations described above it is now possible the get this ratio. In ?? is the NOVAC Evaluation visualized.

Taking the BrO/SO₂ ratio if the column densities are close to zero yields unpredictable and unrealistic results. Thus spectra measured outside of the volcano plume need to be excluded. This could be achieved by setting a BrO or/and a SO₂ threshold. A reasonable BrO threshold need to be at least in the order of the DOAS fit error. But this could lead to elevated BrO/SO₂ ratios, since the BrO error is often close to the detection limit, and thus exclude all low BrO column densities from the evaluation.

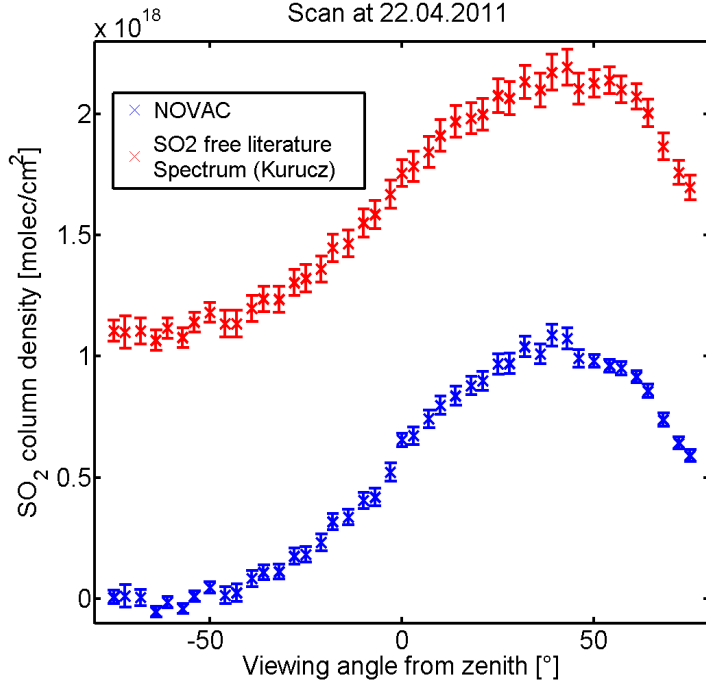


Figure 3.3:

To avoid this problem, an SO₂ threshold of $7 \cdot 10^{17} \frac{\text{molec}}{\text{cm}^2}$ was used to select spectra for the evaluation of the BrO/SO₂ ratio. This threshold is a relatively high SO₂ column density. However, for the lower values of the BrO/SO₂ ratio in this would result in a BrO column density as low as $4 \cdot 10^{13} \frac{\text{molec}}{\text{cm}^2}$, a value only slightly higher than the average DOAS retrieval error for BrO. This approach assures that scans not seeing significant amounts of volcanic gas are filtered out and thus will not significantly influence the BrO/SO₂ ratio. Lübcke et al., 2014

3.2 Contamination Problem

genuine angebane tungurhaua u NEVADO

It might occur that in rare (ca. 10% of the data) scenarios, the volcanic plume covers the whole scan region. This could happen if for example the volcanic plume of the day before still extend over the hole scan area as a consequence of windless conditions. In consequence, the reference is contaminated with volcanic trace gases. Thus the gas amount is underestimated by the NOVAC-Evaluation: In fig. 3.3 we see an example from April 2011 (Tungurahua) where the reference region is contaminated by volcanic trace gases. The blue SO₂ curve shows our calculations with the NOVAC-Evaluation, but since there is still SO₂ in the reference region, therefore the assumption, that the SO₂ amount could be set to zero in the reference region

is wrong. The red curve shows the real SO₂ curve, and we will underestimate the total SO₂ amount of the plume. Contamination occur in approximately 10% of the data.

If the reference region is for any reason contaminated by volcanic trace gases, the reference spectrum has to be replaced by a volcanic-gas-free reference. Alternative spectra are a theoretical solar atlas spectrum (the use of a solar atlas spectrum will be described in section 3.2) or a a volcanic-gas-free reference spectrum recorded by the same instrument.

In the following we will discuss both of these options:

Evaluation using a Solar Atlas Spectrum

An alternative to choose the region with the lowest column density as reference region is to use a theoretical high resolution solar atlas spectrum as reference [Chance and Kurucz \[2010\]](#). The use of a theoretical solar atlas spectrum as a reference which is completely volcanic-trace-gases-free was first proposed by [Lübcke et al. \[2014\]](#). The advantage of using a solar atlas spectrum as reference is, that we know that there are no volcanic trace gases, we do not need to assume, that the minimum SO₂ amount is zero. The disadvantage is, that using a solar atlas spectrum comes along with a drawback of precision: A theoretical solar atlas spectrum is far more precise than the spectra of the NOVAC instruments therefore the instrument functions need to be modeled and added to the retrieval.

The reduction of precision is acceptable for the SO₂ retrieval but not suitable for a BrO retrieval because then most data would be below the detection limit.

Possible contaminations can be checked by a theoretical solar atlas spectrum to evaluate the SO₂ amount in the reference.

Evaluation using a Spectrum of the same Instrument

An alternative reference spectrum could be a a volcanic-gas-free reference spectrum recorded by the same instrument. When using such a reference several problems occur:

As described in chapter 2 the instruments used in NOVAC do not include features like temperature stabilisation due to that the measurements are not independent from external parameters. So we need to choose a reference recorded at similar conditions with respect to meteorology and radiation as well as in the temporal proximity due to instrumental changes with time and ambient conditions. Ideally the external conditions should be equal to the conditions when the plume was recorded.

In this work we will combine both options in order to achieve both, enhanced ac-

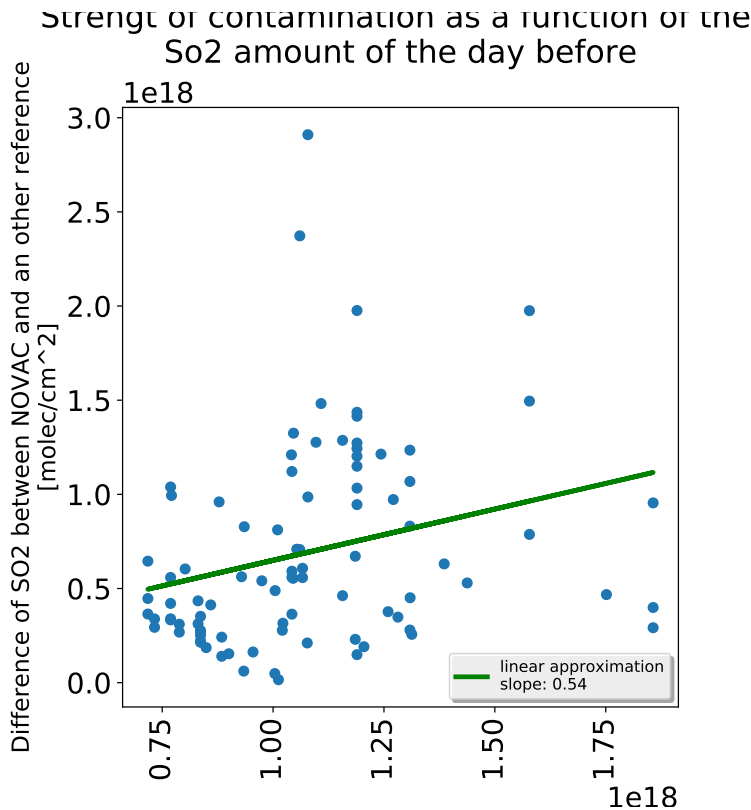


Figure 3.4:

accuracy but still maximum possible precision of the SO₂ and BrO retrievals. So we use the solar atlas spectrum to check for contamination and a reference spectrum recorded in temporal proximity by the same instrument as reference.

In the following we will discuss how to find the an optimal reference from another scan automatically.

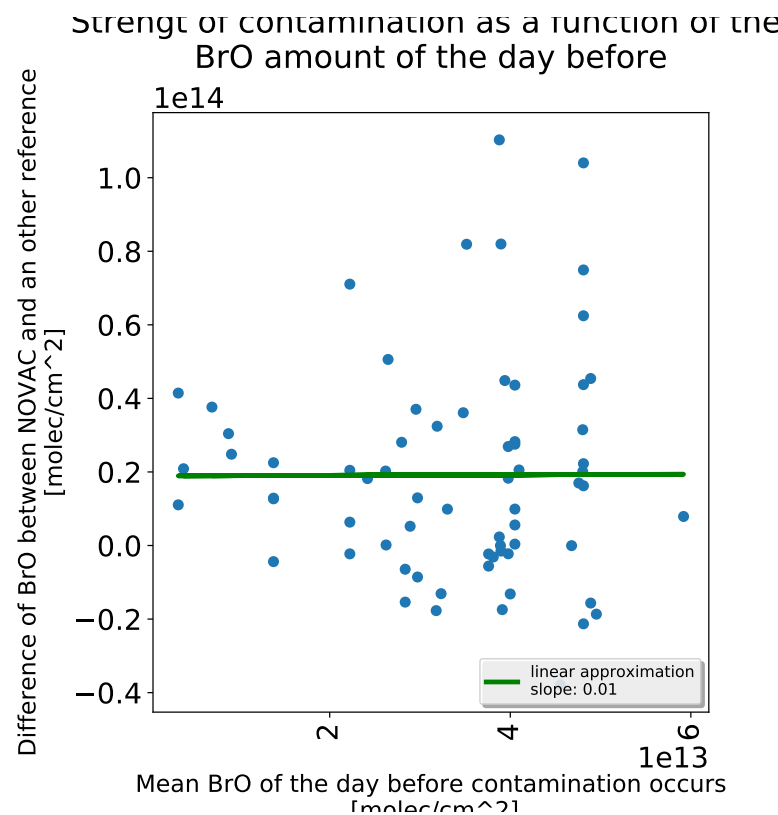


Figure 3.5:

Strength of contamination as a function of the
BrO/SO₂ amount of the day before

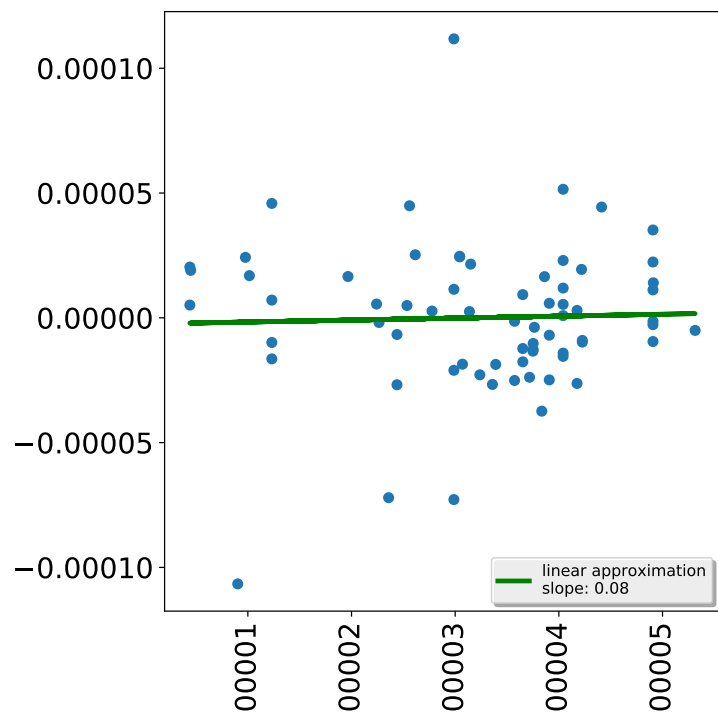


Figure 3.6:

4 Limitations for the evaluation of BrO

Since the SO₂ amount in a volcano plume is rather high (magnitude of SO₂ at Tungurahua $\approx 1e^{18}$, Warnach [2015]) , the evaluation of SO₂ is unproblematic compared to BrO.

Evaluating BrO is more difficult since the amount is much smaller and the measurement error relative to the column density much larger. Since we want to get the BrO/SO₂ we need to maximize the accuracy of BrO. Therefore the aim is to choose the reference with respect to the BrO error, to minimize the BrO Error and to increase the amount of reliable BrO/SO₂ ratio data.

We figured out, that the BrO Error depends strongly on the surrounding conditions when recording the plume and the reference. In the following, we will take a closer look at the dependence of the BrO error on external parameters.

4.1 BrO Error dependence on external parameters

The measurement and evaluation depends on the surrounding conditions like temperature or cloudiness Lübcke [2014]

If choosing a new reference we need to take the surrounding conditions into account. The better the surrounding conditions of the time where the reference is measured coincide with the conditions of the time when the plume is measured, the lower is the BrO error

The surrounding conditions we take into account are temperature, colorindex, exposure time, elevation-angle, daytime and the temporal difference.

In almost all cases (99%) the absolute BrO Error is minimal when using the reference recorded at the same time as the plume spectrum. So we won't be able to get an BrO Error which is smaller than the "Same Time Error".

4.1.1 Time

Due to instrument drifts the fit quality decreases with the time difference between recording the plume and the reference. Therefore it is better to use a reference in temporal proximity.

Figure 4.1 shows the Instrumental drift as a function of time, to create fig. 4.1 we used Tungurahua data, 2008 from June to November. We can observe that the drift changes with time. If we use the reference and plume spectra of the same time, we do not need to care about these effects, since the shift is equal for the plume and reference spectrum, but if the recording time is not the same the quality of the fit changes with the differences in wavelength shift which increases with the time

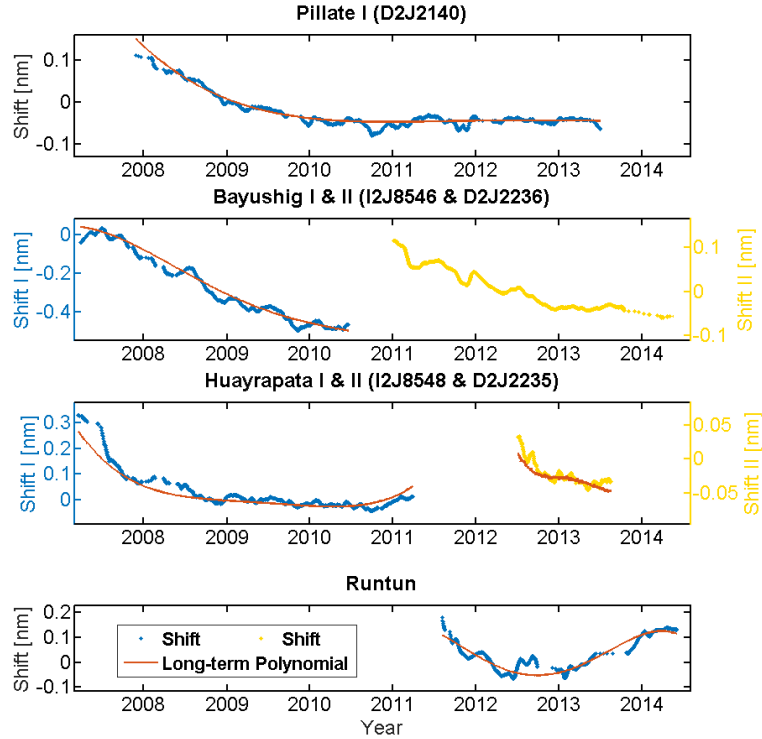


Figure 4.1:

difference.

In fig. 4.3 the BrO Error as a function of the time difference between recording the plume and the reference is shown. The running mean is drawn with a black line. The BrO Error increases with time difference.

To evaluate the maximal time difference, where we still get reliable results we calculated for all possible reference-plume pairs the corresponding BrO Error. With this data we are able to find for all plume spectra the associated reference where the BrO Error is minimal. In ?? a histogram is plotted with the probability of picking the best reference as a function of the time difference. Obviously the best results are if the day of measuring the reference is the same day as measuring the reference that means, if the time difference is smaller than one day. We allow all time difference which are in one sigma area.

We found out that the time interval where it is still reasonable to use references is about 14 days. Therefore we only use references where the recording time difference between plume and reference is smaller than two weeks. When using a references with a temporal difference to the plume of more than 14 days the probability, that the fit quality and thus the BrO error increases to much for our purposes.

4.1.2 Temperature

The Instrument design of the NOVAC instruments compromise between accuracy and longevity as explained in chapter 2. In particular there are no internal thermal stabilizations installed as an attempt to reduce the need for power. This can influence the recorded spectra.

Each pixel of the spectrometer, which is used for the DOAS experiment, collects photons of a certain wavelength range.

The calibration for the wavelength to pixel mapping (WMP) is commonly done with a Mercury lamp or by the comparison with the high defined Kuruz spectrum. As the WMP depends on the optical alignment of the spectrometer, which itself depends on the temperature, it is not constant. Changes in the spectrometers temperature can cause changes in the instrument line function and shifts in the WMP ([Pinardi et al. \[2007\]](#)). Moreover, [Warnach \[2015\]](#) show that, short term shifts are related to the instrument temperature (see Figure 4.4).

The above discussed temperature dependence of the WMP causes a reduction of the fitquality with increasing instrument temperature between plume and reference. Thus the BrO Error increases as well with the temperature difference. To quantify the BrO error dependency on the temperature all plume spectra of Tungurahua from August 2008 to August 2009 (Nevado del Ruiz from to) where evaluated with all plume spectra of the same time. In this time span 1647 "multi-add" spectra from tree different instruments where recorded, so we get approximately 1646^2 plume reference pairs and their corresponding BrO error and temperature. The BrO error as function of the temperature difference can be seen in fig. 4.5. The blue dots shows the mean BrO error at the specific temperature difference, the standard deviation is illustrated with gray bars.

When compare the data of Tungurahua and Nevado Del Ruiz it is noteworthy that the BrO error on temperature dependence of the Data of Nevado Del Ruiz is stronger and the deviation is weaker than at Tungurahua, this may occur due to the larger temperature fluctuation at Nevado Del Ruiz. ?????????? quellen bitte!

When looking at all discussed external parameters, temperature has the strongest impact on the BrO error due to the strong impact on the WMP. [h!]

- The BrO error has the strongest dependence on the temperature difference. At Tungurahua (Nevado Del Ruiz) the BrO error increases by factor of $3.53 \cdot 10^{12}$ per degree.

$$\begin{aligned} \rightarrow BrO_{Error} &= f(ext.P) + 3.53 \cdot 10^{12} \cdot \frac{\Delta T}{1C^\circ} + \mathcal{O}() && Tungurahua \\ \rightarrow BrO_{Error} &= f(ext.P) + 7.56 \cdot 10^{12} \cdot \frac{\Delta T}{1C^\circ} + \mathcal{O}() && NevadoDelRuiz \end{aligned}$$

between monitoring the plume
and reference region

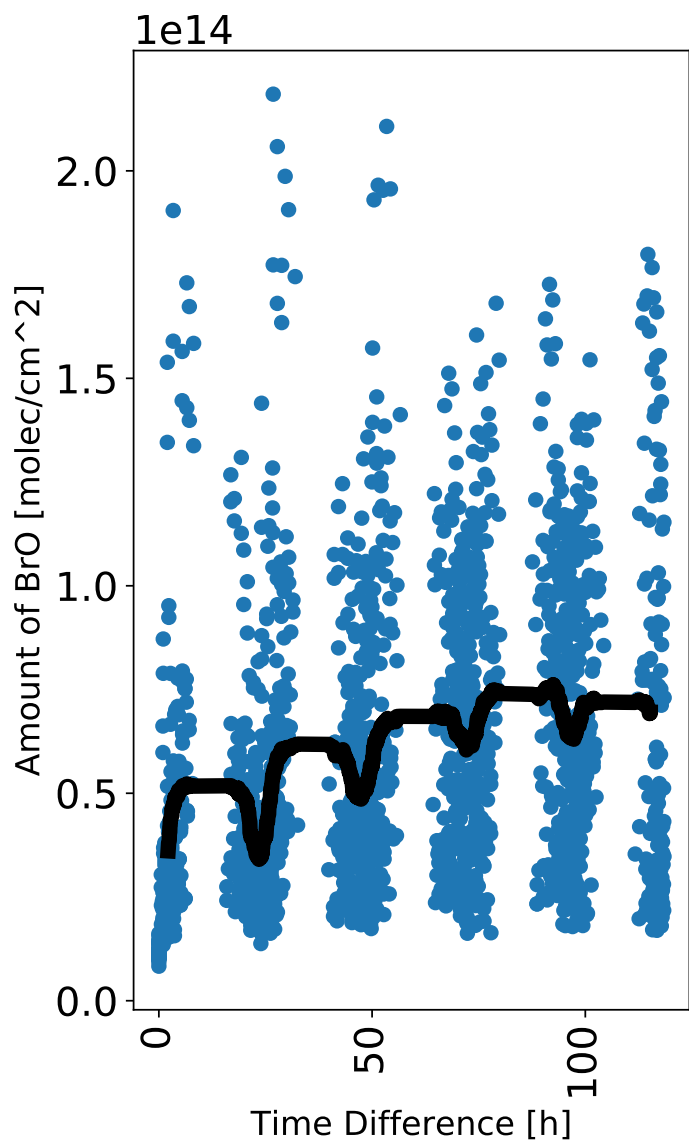


Figure 4.2:

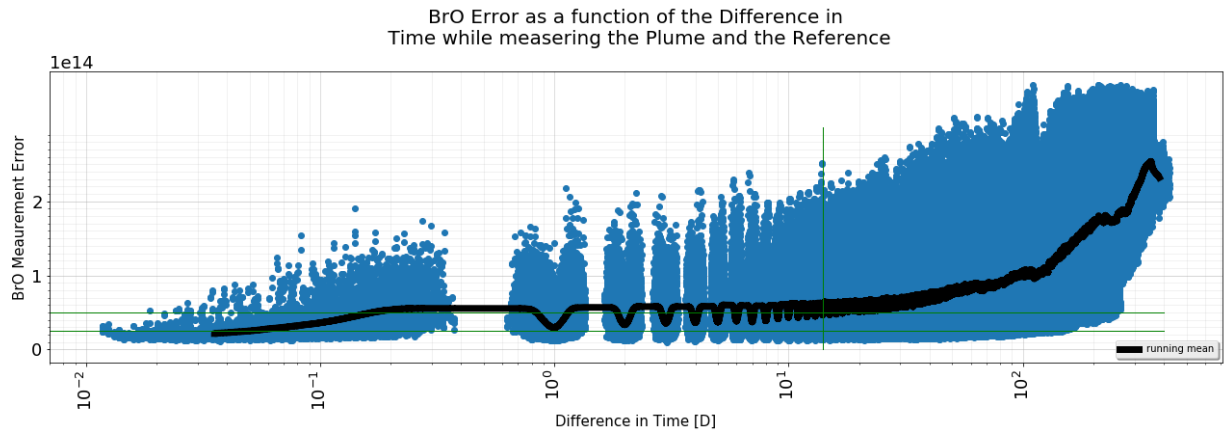


Figure 4.3:

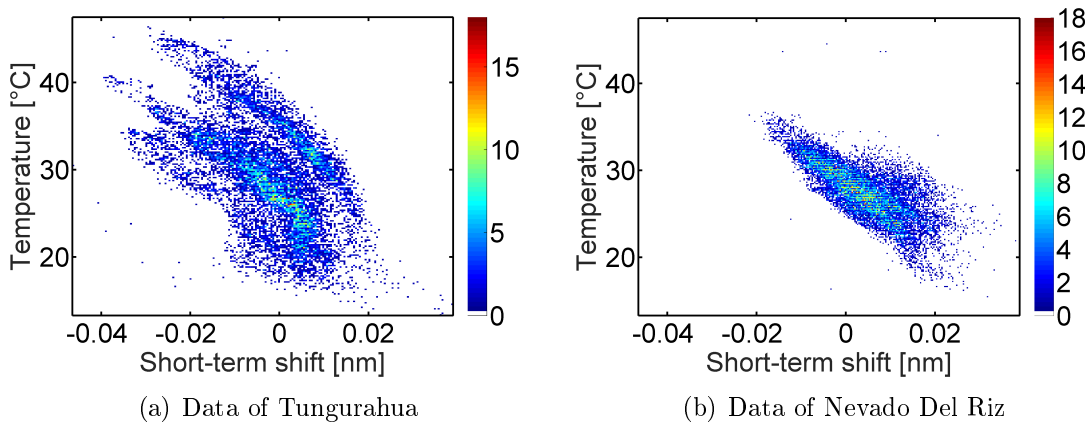


Figure 4.4: Titel unterm gesamten Bild

4.1.3 Daytime

During the day a lot of external parameters like temperature, solar altitude etc. change. In particular the solar altitude could have an impact on the fit quality since the light path of the sun is much longer at the evening than at noon. Figure 4.6 shows the dependency of the BrO error on the daytime. The data are calculated as described for the temperature. As for the temperature the dependence of Nevado Del Ruiz is much larger than of Tungurahua, this might occur during the larger distance from the equator of Nevado Del Ruiz -> besser beschreiben

- We found a dependency of the BrO error on the daytime. We assume, that this dependency comes from other external parameters which change during the day.
- The BrO Error increases with the daytime differences like:

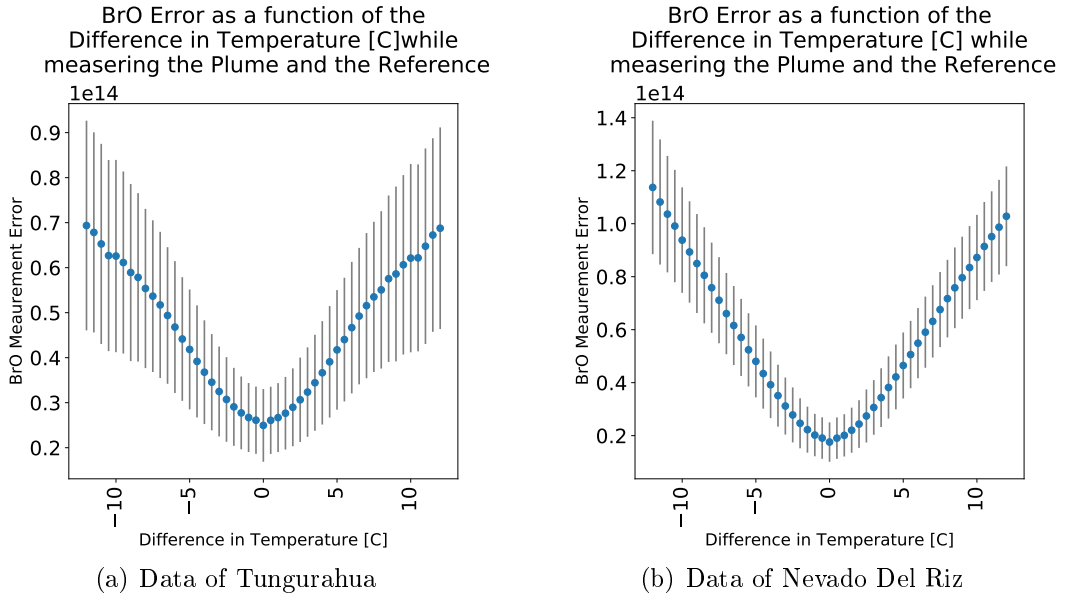


Figure 4.5: Titel unterm gesamten Bild

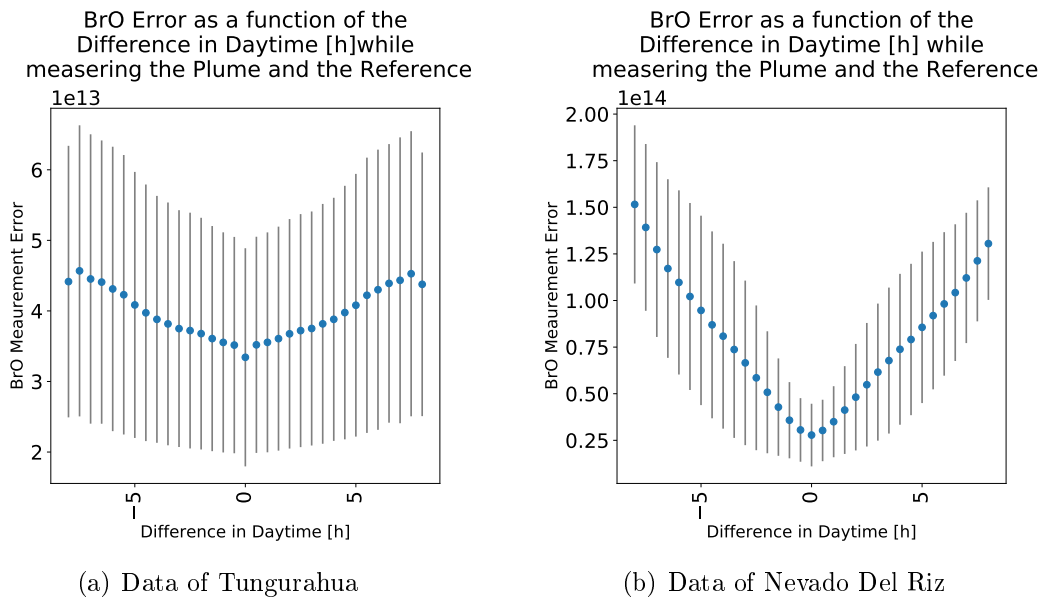


Figure 4.6: Titel unterm gesamten Bild

$$\rightarrow BrO_{Error} = f(ext.P) + 1.33 \cdot 10^{12} \cdot \frac{\Delta DT}{1h} + \mathcal{O}() \quad Tungurahua$$

$$\rightarrow BrO_{Error} = f(ext.P) + 1.58 \cdot 10^{13} \cdot \frac{\Delta DT}{1h} + \mathcal{O}() \quad NevadoDelRuiz$$

4.1.4 Colorindex

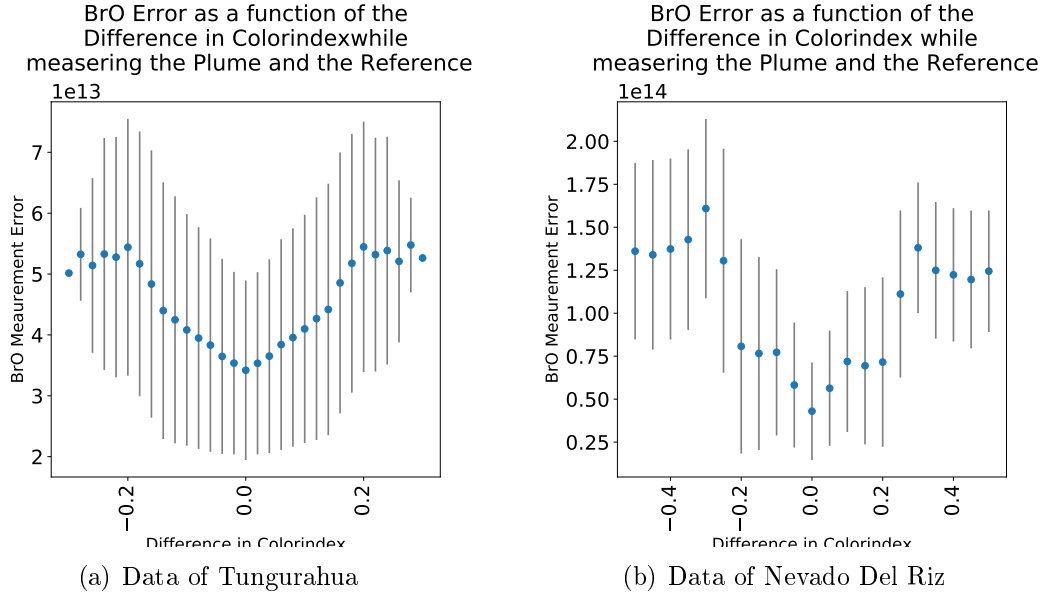


Figure 4.7: Titel unterm gesamten Bild

Clouds have a strong influence on the atmospheric radiative transfer and thus affect the interpretation and analysis of DOAS - observations Wagner et al. [2014].

Clouds can be identified by several measurement quantities that they influence. As Mie scattering is dominant in clouds the wavelength of the light that is scattered is different than the Rayleigh sky. Thus, clouds can be easily identified by their white color. Therefore, the cloudiness of the sky can be quantified in a scalar measure defined by the ratio of the measured intensity at two wavelengths, the so-called colour index. Wagner et al. [2014] showed that for a zenith-looking instrument the measured radiation intensity is enhanced by clouds. Thus, clouds can cause large errors for the retrieved gas column density and the corresponding uncertainties. Cloud effects are especially severe if the cloudiness for the recorded plume and reference spectra strongly defer. Also for broken clouds the described effect can be observed as measurements at some elevation angles might be influenced by clouds while others are not. In this work the Colour Index (CI) is the ratio between the intensities at 320nm and 360 nm. These two wavelengths are as far apart as the filter used for stray-light prevention in the spectrometers allows. On the other hand, the lower wavelength avoids the deep UV range where SO₂ and O₃ absorption plays a dominant role. The Mie scattering in the clouds is responsible for the higher amount of radiation from larger wavelengths. This results in a decrease of the CI (Lübecke [2014]).

We evaluated the CI at the zenith, to increase the stability of the fit we added in each cases 10 intensitys. Using always the zenith to evaluate the colour index makes

the colour index more comparable, but if broken clouds occur, the CI of the reference and the plume could differ from the calculated CI of the zenith. This could be a reason for the large deviations of the mean BrO error as function of the colour index (see fig. 4.7)

- The BrO Error increases with the Colorindex differences as

$$\rightarrow BrO_{Error} = f(ext.P) + 1.01 \cdot 10^{13} \cdot \frac{\Delta Cidx}{0.1} + \mathcal{O}() \quad Tungurahua$$

$$\rightarrow BrO_{Error} = f(ext.P) + 4 \cdot 10^{13} \cdot \frac{\Delta Cidx}{0.1} + \mathcal{O}() \quad NevadoDelRuiz$$

4.1.5 Elevation Angle

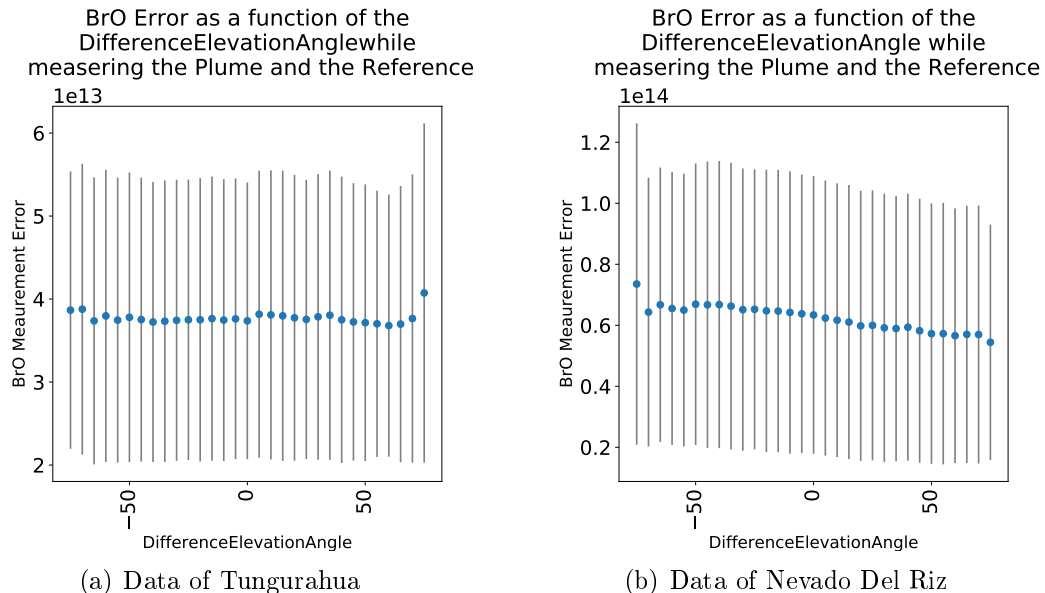


Figure 4.8: Titel unterm gesamten Bild

The elevation angle describes the angle between the horizon and the zenith. When using the plume spectrum and the reference spectrum of the same time, the difference in elevation angle cannot be zero, since the plume is always somewhere else than the reference located.

The BrO error doesn't depend significantly on the difference between the Elevation Angles. This could have several reasons. One problem is, that the Elevation Angle of Plume and Reference spectrum is not the same. This could also be a reason of uncertainty of the evaluations of the plume spectrum.

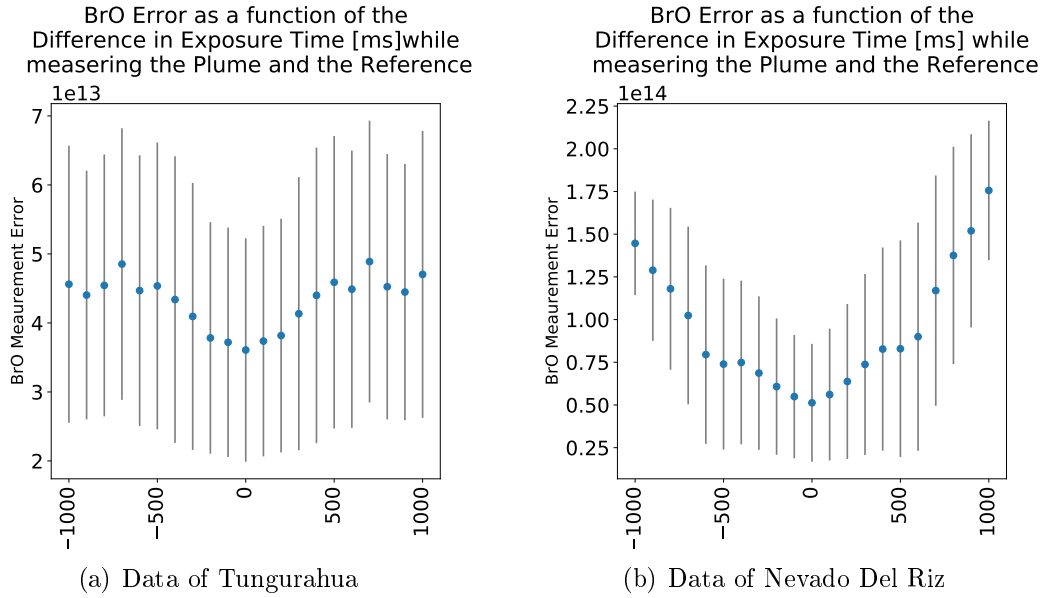


Figure 4.9: Titel unterm gesamten Bild

4.1.6 Exposure Time

The Exposure Time is a degree of sky lightness. The exposure time is the length of time the sensor of the NOVAC instrument is exposed to light. The amount of light that reaches the film or image sensor is proportional to the exposure time. The exposure time is adjusted in the way that the maximum intensity does not overly the capacity of the sensor.

We can observe a small dependency of the BrO error on the Exposure time at Tungurahua and Nevado Del Ruiz as it is shown in fig. 4.9

- The BrO Error increases with the exposure time differences as

$$\rightarrow BrO_{Error} = f(ext.P) + 1.92 \cdot 10^{12} \cdot \frac{\Delta ET}{10^{-2}s} + \mathcal{O}() \quad \text{Tungurahua}$$

$$\rightarrow BrO_{Error} = f(ext.P) + 1.0 \cdot 10^{13} \cdot \frac{\Delta T}{10^{-2}s} + \mathcal{O}() \quad \text{NevadoDelRuiz}$$

5 Method

Based on the findings about the influence of external parameters on the BrO error we developed an algorithm which is able to pick an appropriate volcanic-trace-gas free reference.

The first step is, to evaluate every reference with solar atlas spectrum, to check for contamination. A Spectrum is treated as contaminated if the SO₂ column density of the reference (evaluated with a solar atlas spectrum) is larger as $2 \cdot 10^{17} \frac{\text{molec}}{\text{cm}^2}$.

If the reference is contaminated:

- We have a list of possible references where all references are not contaminated and the temporal distance to the plume date is no longer than 14 days.
- we calculate of all possible references the differences in the external parameters
- We use the analysis of external parameters described above to estimate the BrO error of all references
- We choose the reference with the smallest estimated BrO error as new reference
- We evaluate the plume spectra with the new reference.

The assumption is, that the BrO error ϵ_{BrO} can be described as the sum of ϵ_0 and the deviation of ϵ_{BrO} with respect to all external parameters. ϵ_0 is the BrO error when evaluate the plume spectrum with the "same-time-reference", it is determined due to the accurateness of the NOVAC-instruments.

$$\epsilon_{BrO} = \epsilon_0 + \frac{d\epsilon}{dt} + \frac{d\epsilon}{d^\circ} + \frac{d\epsilon}{dT} + \frac{d\epsilon}{ddt} + \frac{d\epsilon}{dc} + \mathcal{O}(OE) \quad (5.1)$$

$$\rightarrow \Delta\epsilon_{BrO} = \epsilon_{BrO} - \epsilon_0 = \frac{d\epsilon}{dt} + \frac{d\epsilon}{d^\circ} + \frac{d\epsilon}{dT} + \frac{d\epsilon}{ddt} + \frac{d\epsilon}{dc} + \mathcal{O}(OP) \quad (5.2)$$

With ϵ_{BrO} describes the BrO Error, t: time between plumetime and referencetime, T, temperaure; dt: daytime, c: colorindex, OP: other excluded external parameters
The task occurring at this stage is to find the best representation for the deviations.
An then find the reference which minimize $\Delta\epsilon_{BrO}$

The easiest way is to just calculate the BrO error of all possible references for every plume. Using this method we would be able to just choose the reference where the BrO error is minimal. But this takes to much time since the evaluation would be proportional to the number of possible references because the evaluation need to be done for every plume-reference pair. Doing the evaluation for every plume-reference

pair would make it impossible to do the evaluation in real, or near real time. But we use this optimal evaluation to rate our model and compare them among each other. The optimal evaluation always choose the reference with the smallest absolute error. We don't use the relative error due to his vulnerability. Using the relative error could lead to a less preciseness.

Hier ein Bild, das eine Plume gegen viele referencen auswertet und hier die Abweichungen zeigt

The results of the algorithm which chooses the reference automatically are described relative to an optimal evaluation. If the relative error is larger than 5 we don't use the data.

We tried several methods for choosing the best reference based on the analysis of external parameters. Fitting the data with a first order polynomial brought the best results.

5.1 Fit data

When looking at the analysis of the external parameters (see fig. 4.5-4.9) we can observe curves which are symmetric to the zero position. Therefore we conclude that it makes no difference whether the difference of a specific external parameter is positiv or negativ. Thus we take the absolute values for our calculations.

If we assume that all differentiations are linear, than we can write eq. (5.2) as:

$$\Delta\epsilon_{BrO} = a_t \cdot \Delta t + a_\circ \cdot \Delta^\circ + a_T \cdot \Delta T + a_{dt} \cdot \Delta dt + a_c \cdot \Delta c + \mathcal{O}(OP) \quad (5.3)$$

We used the same data as in fig. 4.5-4.9 to get the coefficients a_x of eq. (5.3). We used on ordinary least square linear regression to get the coefficients a_x . In particular we used the python function LinearRegression from the library `sklearn SKl`.

The constants for Tungurahua and Nevado Del Ruiz are:

- Plume data are reliable if the SO₂ column density is larger as $7 \cdot 10^{17} \frac{\text{molec}}{\text{cm}^2}$
- Data are above the detection limit if the column density as two times larger than the fit error.
- If the reference is contaminated:

(a) Data of Nevado Del Riz D2J2201_0		
Constant	value	importance
a_T	7.338e+12	0.840
a_{ET}	1.545e+10	0.045
a_t	-2.6e+09	0.0
a_{dt}	1.805e+12	0.091
a_c	2.301e+13	0.031

(b) Data of Nevado Del Riz D2J2200_0		
Constant	value	importance
a_T	1.162e+13	0.908
a_{ET}	2.811e+10	0.046
a_t	-1.7e+09	0.0
a_{dt}	1.076e+12	0.034
a_c	3.587e+13	0.016

(c) Data of Nevado Del Both Instruments		
Constant	value	importance
a_T	1.073e+13	0.973
a_{ET}	3.478e+10	0.070
a_t	-9.1e+08	0.0
a_{dt}	1.523e+11	0.006
a_c	-6.811e+13	-0.047

Table 5.1: (a)Data from Nevado Del Ruiz from the D2J2201_0 instrument. All external parameter where taken into account. $\epsilon_0 = 5.404e+12$ (b)Data from Nevado Del Ruiz from the D2J2200_0 instrument. All external parameter where taken into account. $\epsilon_0 = 1.105e + 13$ (c) Data from Nevado Del Ruiz from both instrument. All external parameter where taken into account. $\epsilon_0 = 1.260e + 13$

percentage of correlated data
function of the minimum SO₂ amo_l

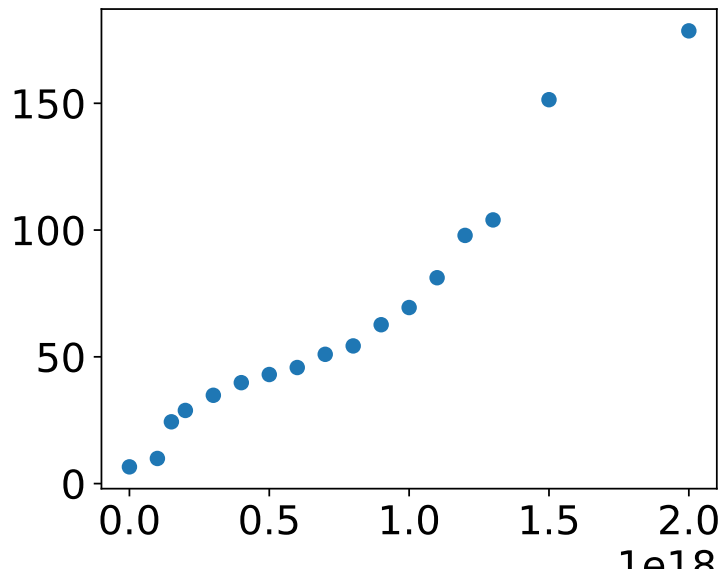


Figure 5.1:

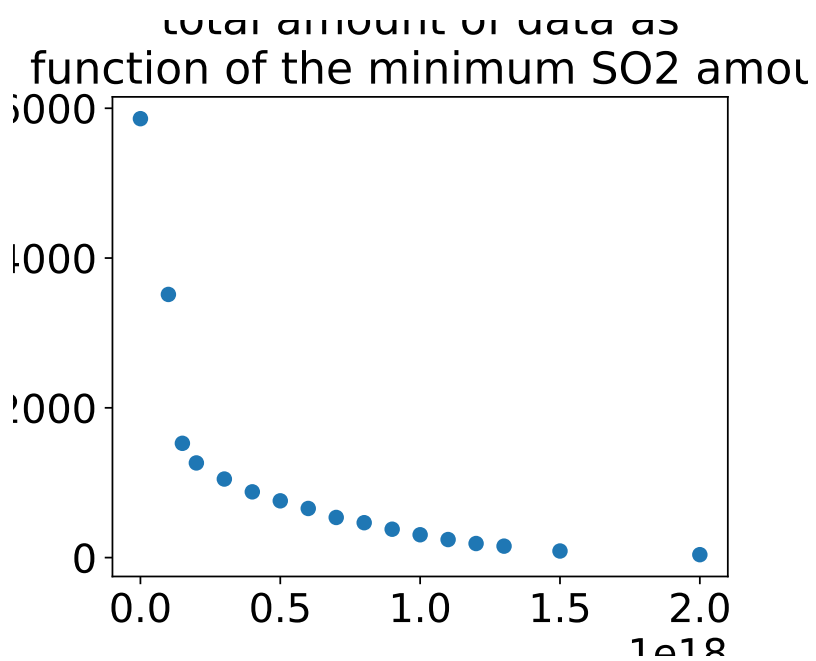


Figure 5.2:

		Error	Amount of Data	valid data
All Variables	independent	1.51	95%	10,5%
	dependent	1.40	98%	8%
Exposure Time	independent	1.47	97%	10%
	All	1.39	98%	7%
Exp.Time u Coloridx	independent	1.40	98%	11
	All	1.35	98%	7%

Evaluation of all contaminated data from Nevado Del Ruiz

Instrument	Dev from opt eval. (mean/median)	valid data
D2J2201_0	1.14 / 0.82293	128/283 = 45.2%
D2J2200_0	1.5 / 0.89965	954/1109 = 86.0%
Both	1.26/0.847	1073/1392 = 77.1%

Table 5.2: Data from Nevado Del Ruiz from the D2J2201_0 instrument. All external parameter where taken into account. $\epsilon_0 == 5.404e + 12$

5.2 Other approaches

- In the optimal results are 15% valid data
- We also tried other possibilities than fitting to find the reference where the BrO error is minimal. In the following we present two additional possibilities but compared to fitting the results are not as good.

5.2.1 Nearest neighbours

- Description of the Nearest Neighbours Method

Nearest neighbor search (NNS), as a form of proximity search, is the optimization problem of finding the point in a given set that is closest (or most similar) to a given point. Closeness is typically expressed in terms of a dissimilarity function: the less similar the objects, the larger the function values. Formally, the nearest-neighbor (NN) search problem is defined as follows: given a set S of points in a space M and a query point $q \in M$, find the closest point in S to q. Donald Knuth in vol. 3 of *The Art of Computer Programming* (1973) called it the post-office problem, referring to an application of assigning to a residence the nearest post office. A direct generalization of this problem is a k-NN search, where we need to find the k closest points. Most

commonly M is a metric space and dissimilarity is expressed as a distance metric, which is symmetric and satisfies the triangle inequality. Even more common, M is taken to be the d -dimensional vector space where dissimilarity is measured using the Euclidean distance, Manhattan distance or other distance metric. However, the dissimilarity function can be arbitrary. One example are asymmetric Bregman divergences, for which the triangle inequality does not hold.

5.2.2 Iterative

- Description of the iterative Method

The idea of the iterative method was, that the importance of the individual external parameters are very different, that means if we have the list of possible references, we took all references where the temperature difference is minimal, so we get a new, much smaller list of possible references. From this list we choose all references where the next external parameter for example the daytime is minimal and get again a new list. We proceed this way with the following external parameters. We experiment with the sequence of the parameters, to increase the success of the method. The final sequence was:

Temperature •

6 Comparison with NOVAC Evaluation

We want to

- Results only for contaminated data
 - Difference in SO₂ data evaluated with NOVAC-method and contamination-based evaluation
 - Difference in BrO data evaluated with NOVAC-method and contamination-based evaluation
 - Difference in BrO/So₂ Ratio data evaluated with NOVAC-method and contamination-based evaluation
- Amount of BrO data more than before (valid and not valid and above detection limit)
- Amount of SO₂ data more than before (valid and not valid and above detection limit)
- Amount of BrO/SO₂ data more than before (valid and not valid and above detection limit)
- More BrO data: 51%
- More valid BrO data: 38%
- Compare the daily means: how many more data? due to higher S0₂ values
-

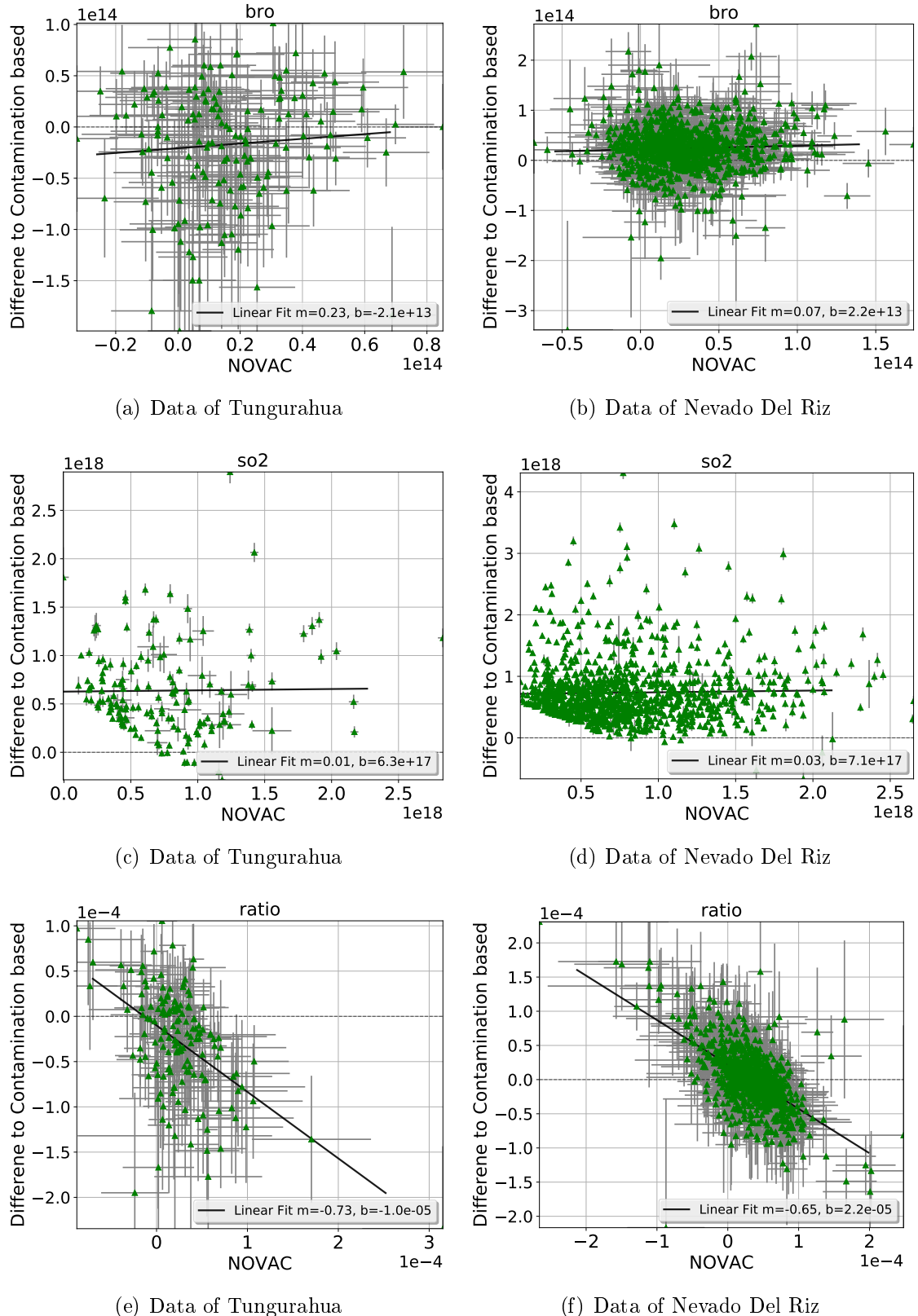


Figure 6.1: The dependency of the Difference between contamination based data and NOVAC to the data evaluated with the NOVAC data

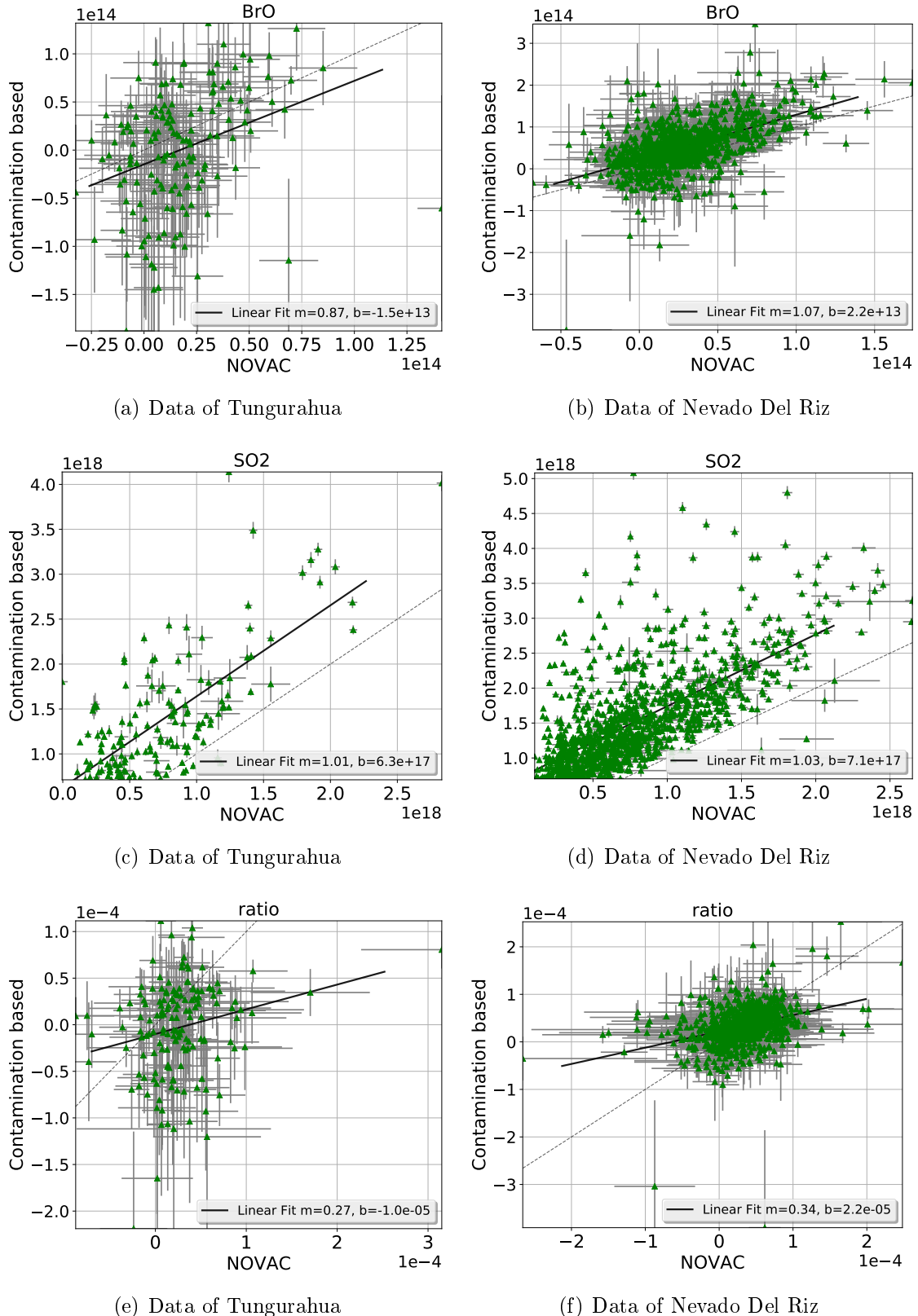


Figure 6.2: The dependency of the Difference between contamination based data and NOVAC to the data evaluated with the NOVAC data

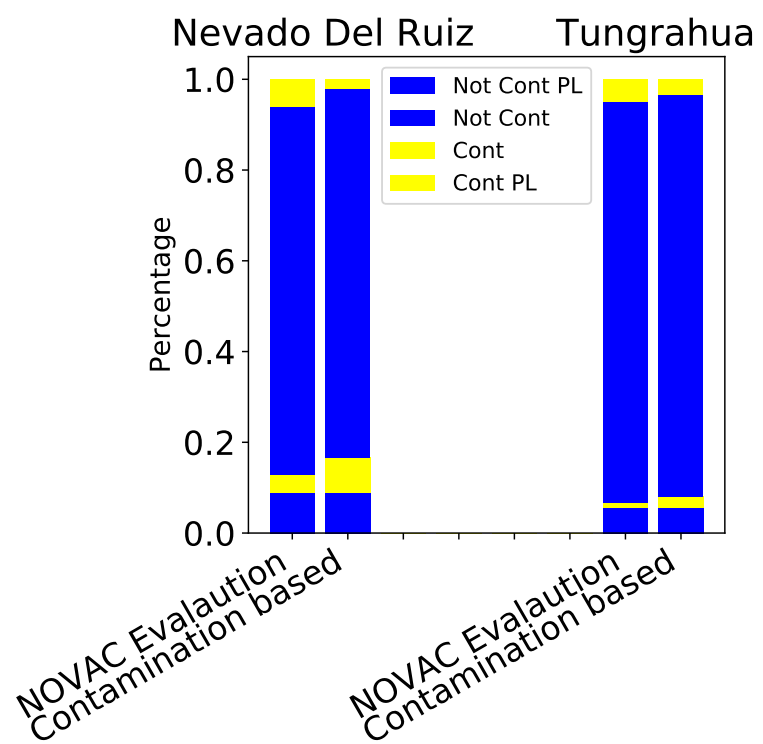


Figure 6.3:

7 Results

Interpretation of the BrO/SO₂ ratio time-series

7.1 Tungurahua

<i>MengeanDateninsgesamt :</i>	5883	≡	1
<i>Davon : (NOVACAuswertung)berplumelimit</i>	712	≡	0.121
<i>Davon : MengeanDaten, dienichtKontaminiertsind :</i>	5504	≡	0.936
<i>DavonimPlume – limit :</i>	599	≡	0.102
<i>DavonberdemDetectionLimit :</i>	36	≡	0.006
<i>Davonsindkontaminiert :</i>	379	≡	0.064
<i>Davon(mitNOVacaausgewertet)berplumelimit :</i>	114	≡	0.301
<i>Davon(NeueAuswertung)berplumelimit</i>	185	≡	0.488

Dh in den kontaminierten daten sind mit NOVAC ausgewerteten daten 2.485 häufiger über dem plume limit

7.2 Nevado Del Ruiz

<i>MengeanDateninsgesamt :</i>	8962	≡	1
<i>Davon : (NOVACAuswertung)berplumelimit</i>	142	≡	0.016
<i>Davon : nichtkontaminiertedaten :</i>	8596	≡	0.959
<i>DavonimPlume – limit :</i>	123	≡	0.014
<i>DavonberdemDetectionLimit :</i>	53	≡	0.006
<i>Davonsindkontaminiert :</i>	366	≡	0.041
<i>Davon(mitNOVacaausgewertet)berplumelimit :</i>	20	≡	0.055
<i>Davon(NeueAuswertung)berplumelimit</i>	179	≡	0.489

Dh in den kontaminierten daten sind mit NOVAC ausgewerteten daten 3.449 häufiger über dem plume limit

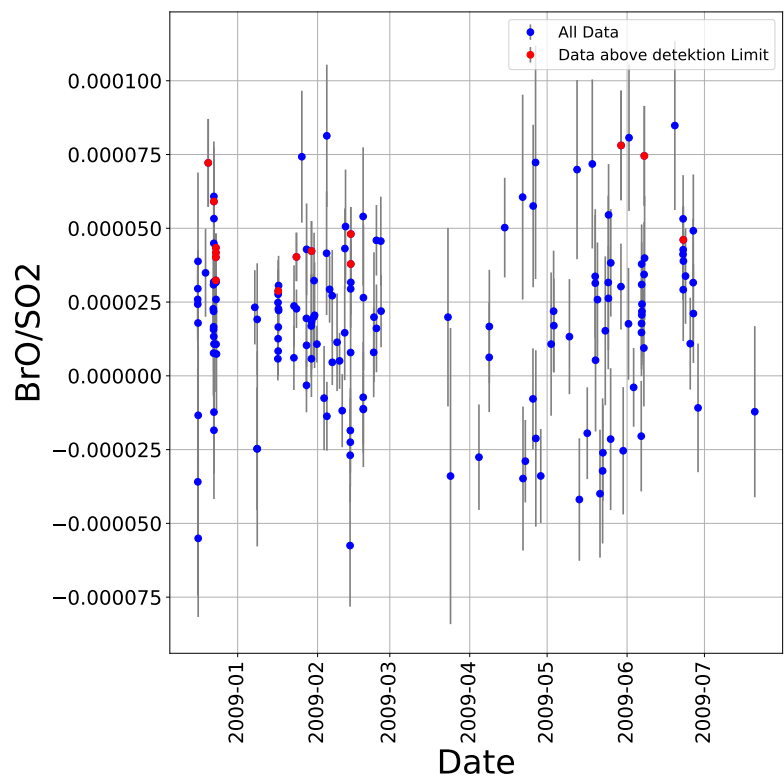


Figure 7.1:

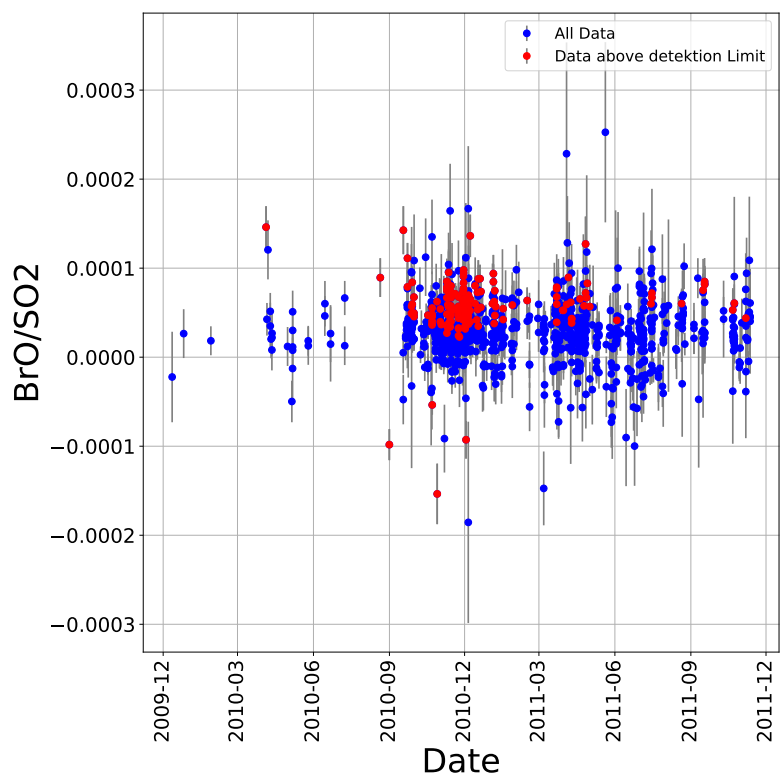


Figure 7.2:

8 Issues of our method

8.1 Contamination of the plume

- As discussed above it might occur, that, that the reference is contaminated for example by the plume of the day before. If that happens, we underestimate the gas amount by using a contaminated reference. But another possibility is, that the plume is also contaminated. This might be the case if the volcanic gas of the volcano is not taken away by the wind, but accumulates in the plume. If this is the case, using an other reference would lead to an overestimation of the column density of gases.

9 Conclusion

....

Part III

Appendix

A Lists

A.1 List of Figures

1.1	14
1.2	17
1.3	17
1.4	21
1.5	30
2.1	Global map of the volcanoes monitored by NOVAC. Used with friendly permission of Santiago Arellano.	32
2.2	Titel unterm gesamten Bild	33
2.3	34
3.1	35
3.2	Titel unterm gesamten Bild	36
3.3	37
3.4	39
3.5	40
3.6	41
4.1	43
4.2	45
4.3	46
4.4	Titel unterm gesamten Bild	46
4.5	Titel unterm gesamten Bild	47
4.6	Titel unterm gesamten Bild	47
4.7	Titel unterm gesamten Bild	48
4.8	Titel unterm gesamten Bild	49
4.9	Titel unterm gesamten Bild	50
5.1	54
5.2	54
6.1	The dependency of the Difference between contamination based data and NOVAC to the data evaluated with the NOVAC data	58
6.2	The dependency of the Difference between contamination based data and NOVAC to the data evaluated with the NOVAC data	59
6.3	60

7.1	62
7.2	63

A.2 List of Tables

5.1 (a) Data from Nevado Del Ruiz from the D2J2201_0 instrument. All external parameter where taken into account. $\epsilon_0 == 5.404e + 12$
 (b) Data from Nevado Del Ruiz from the D2J2200_0 instrument. All external parameter where taken into account. $\epsilon_0 == 1.105e + 13$
 (c) Data from Nevado Del Ruiz from both instrument. All external parameter where taken into account. $\epsilon_0 = 1.260e + 13 \dots \dots \dots$ 53

5.2 Data from Nevado Del Ruiz from the D2J2201_0 instrument. All external parameter where taken into account. $\epsilon_0 == 5.404e + 12 \dots \dots \dots$ 55

B Bibliography

Python scikit-learn.org. http://scikit-learn.org/stable/modules/generated/sklearn.linear_model.LinearRegression.html. Accessed: 2018-01-19.

K Chance and RL Kurucz. An improved high-resolution solar reference spectrum for earth's atmosphere measurements in the ultraviolet, visible, and near infrared. *Journal of quantitative spectroscopy and radiative transfer*, 111(9):1289–1295, 2010.

Peter Lübcke. *Optical remote sensing measurements of bromine and sulphur emissions: Investigating their potential as tracers of volcanic activity*. PhD thesis, 2014.

Peter Lübcke, Nicole Bobrowski, S Arellano, Bo Galle, G Garzón, Leif Vogel, and U Platt. Bro/so 2 molar ratios from scanning doas measurements in the novac network. *Solid Earth*, 5(1):409, 2014.

G Pinardi, MV Roozendael, and C Fayt. The influence of spectrometer temperature variability on the data retrieval of so2. *NOVAC second annual activity report, NOVAC consortium*, 44:48, 2007.

U Platt and N Bobrowski. Quantification of volcanic reactive halogen emissions. *Volcanism and Global Change*, eds A. Schmidt, K. Fristad, L. Elkins-Tanton, Cambridge University Press, Cambridge, UK, ISBN, 1466525386, 2015.

Ulrich Platt and Jochen Stutz. Differential absorption spectroscopy. *Differential Optical Absorption Spectroscopy*, pages 135–174, 2008.

A Schmidt and A Robock. Volcanism, the atmosphere and climate through time. *Volcanism Glob. Environ. Chang*, pages 195–207, 2015.

Anja Schmidt, Kirsten Fristad, and Linda T Elkins-Tanton. Volcanism and global environmental change, 2015.

Hans-Ulrich Schmincke. *Vulkanismus*. Wissenschaftliche Buchgesellschaft, 3 edition, 2000.

S Solomon, RW Portmann, RR Garcia, W Randel, F Wu, R Nagatani, J Gleason, L Thomason, LR Poole, and MP McCormick. Ozone depletion at mid-latitudes: Coupling of volcanic aerosols and temperature variability to anthropogenic chlorine. *Geophysical research letters*, 25(11):1871–1874, 1998.

Thorvaldur Thordarson and Stephen Self. Atmospheric and environmental effects of the 1783–1784 laki eruption: A review and reassessment. *Journal of Geophysical Research: Atmospheres*, 108(D1), 2003.

T Wagner, A Apituley, S Beirle, S Dörner, U Friess, J Remmers, and R Shaiganfar. Cloud detection and classification based on max-doas observations. *Atmospheric Measurement Techniques*, 7(5):1289–1320, 2014.

Simon Warnach. Improvements of bro and so2 retrievals of novac data - tungurahua volcano as a case study. Master’s thesis, 2015.

Erklärung:

Ich versichere, dass ich diese Arbeit selbstständig verfasst habe und keine anderen als die angegebenen Quellen und Hilfsmittel benutzt habe.

Heidelberg, den (Datum)